

Search For Single Top Quark Production Optimized for s-channel Production With SecVtx + JetProb b-tag Method

Koji Nakamura¹, Shinhong Kim

University of Tsukuba

Abstract

This note describe s-channel-optimized search for single top quark production using 1.9 fb^{-1} of data accumulated with the CDF detector. This note reports the first result of the s-channel optimized search. We are using events with one high- P_T lepton, large missing E_T and two b-quark-identified jets where one jet is identified using secondary vertex tagger(SecVtx) and the other jet is identified using SecVtx or jet probability tagger(JetProb). In this analysis we have developed a kinematics fitter and a likelihood-based separator between signal and background.

As a result, no evidence is seen for single-top quark s-channel production. The 95 % CL. upper limit for the s-channel production cross section is $\sigma_s = 2.35 \text{ pb}$.

¹kojin@fnal.gov

Contents

1	Introduction	3
2	EventSelection and Background Estimation	4
2.1	Data and Monte Carlo Samples	4
2.2	Event Selection and Expected Number of Events	4
2.3	two b-tag method using SecVtx and JetProb Tagger	4
2.4	Non-W Modeling for PHX electron (anti-PHX and jet-electron comparison)	4
2.5	effect of QCD cut removal and non-W modeling	5
3	S-channel Optimized Kinematic Fitter	10
3.1	Kinematics Fitter	10
3.2	Likelihood for b-jet from top decay	14
3.3	B-jet Energy Correction	15
4	Likelihood-based separator of signal from background	17
5	Systematic Uncertainties	22
5.1	Rate Uncertainties	23
5.2	Shape Uncertainties	24
6	Expected Sensitivity and Hypothesis Test	25
7	Result with CDF II Data	26
8	Conclusions	26
A	Background Estimation table	29
B	input variables	38

1 Introduction

Top quark has a weak isospin $1/2$ composing a weak isospin doublet with a bottom quark. It predict not only top quark pair production via strong interaction but also singly produced together with a bottom quark via weak interaction. However, finding single top quark production is challenging since it is rarely produced ($\sigma_{\text{singletop}} = 2.9 \text{ pb}$) against background processes with the same final state like $W + \text{jets}$ and $t\bar{t}$. Since the signal to background ratio is small, we need a better discrimination of signal and background events which can be achieved by using more information to characterize each event. The typical processes of single top quark production at the Tevatron are illustrated in Figure 1. In our search, events with a leptonic decaying W boson and exactly two tight jets. Now three kinds of analyses are reporting evidence for electroweak single top quark production using 2.2 fb^{-1} of CDF II data collected between 2002 and 2007[1] [2] [3]. The combination of these three analyses, 4.7σ sensitivity is expected. The observed excess reached 3.7σ . It is really close to the observation.

This note describes the first result of single top quark search optimized to s-channel production. This search is really promising to help the observation since the current analyses are optimized to t-channel production. As a further motivation, the s-channel cross section is enhanced or suppressed by non-standard model particle like W' or Heavy charged Higgs boson. These particles can be seen directly as a mass resonance of a top quark and bottom quark. Most events of the t-channel final state have only one b-jet however the s-channel final state events have two b-jets. Two b-jets final state helps to separate s-channel signal from t-channel. In addition this final state is exactly the same as the standard model Higgs boson produced in association with a W boson, where Higgs decays to $b\bar{b}$.

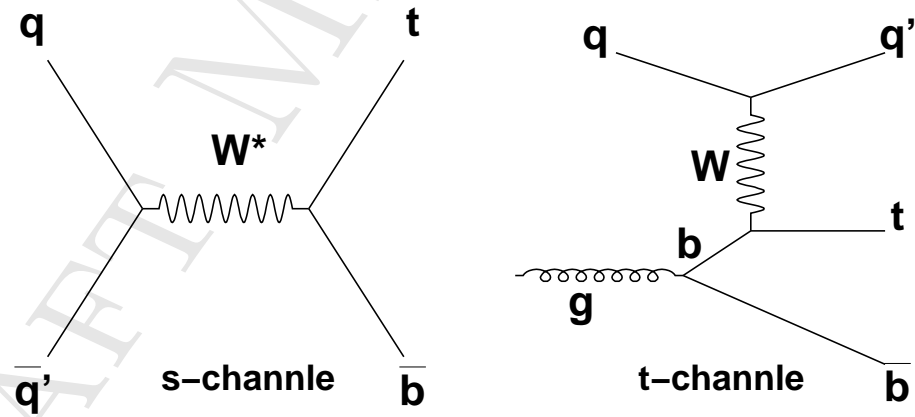


Figure 1: Typical processes of single Top quark production at the Tevatron.

2 EventSelection and Background Estimation

2.1 Data and Monte Carlo Samples

The same as singletop the other analyses.

2.2 Event Selection and Expected Number of Events

Candidate events for this analysis are selected by requiring a $W + 2\text{jets}$ event topology where W decays leptonically, $W \rightarrow e\nu_e$ or $W \rightarrow \mu\nu_\mu$. Both of the two jets should be identified as a b-jet using SecVtx or JetProb tagging algorithm. We will describe our two b-jet tag later.

The detailed event selection and the estimate strategy has been performed and summarized in a separate CDF note [4][5]. We use mostly the same event selection as Method II in [6], except for the following : 1) To increase statistics we did not apply the QCD cut, 2) we used anti-electron sample for PHX non-W estimation instead of jet-electron. We will also discuss these two points later.

Table 1 lists the expected event yield for $W+2\text{-btagged jets}$ events. For the MC based background ($WW, WZ, ZZ, t\bar{t}, t - \text{channel}$ and $Z+\text{jets}$) and signal($s - \text{channel}$), the estimates of uncertainty only cover uncertainty on the event detection efficiency which is defined in [4]. The lists of the expected event yield for each b-tagging categories and each detectors show in the appendix.

2.3 two b-tag method using SecVtx and JetProb Tagger

There is a large amount of the background in the $W+2\text{jet}$ bin, and more than half of them come from non-b-jet background for the at least one SecVtx b-tag category. Two b-tag method reduces these non-b-jet background, but decrease the tagging efficiency. So To improve this efficiency, after requiring one SecVtx tag, apply SecVtx b-tag or JetProb($\text{JP} < 5\%$) b-tag for the other jet. Second jet tagging efficiency in SecVtx double tag category(SV&&SV) is 23.4%. Second jet tagging efficiency with JetProb tag excluding SV&&SV category is 19.2%. Included JetProb tag as a second jet b-tagger, acceptace of the signal increased by about 82% from SecVtx double tag.

2.4 Non-W Modeling for PHX electron (anti-PHX and jet-electron comparison)

The non-W shape is derived from anti-PHX electron, which passes all cuts on the kinematic variables but fails at least two cuts on identification variables out of five as listed in Table 2. We compared the anti-PHX template shape and the jet-electron shape as shown in Figure 3 (singletop group are using jet-electron template currently). The anti-PHX template has higher missing E_T tail than the jet-electron template.

Process	2jets	3jets	4jets	5jets
s-channel	11.7 ± 2.0	4.2 ± 0.7	1.0 ± 0.2	0.2 ± 0.0
t-channel	2.7 ± 0.5	3.4 ± 0.6	1.0 ± 0.2	0.2 ± 0.0
WW	1.1 ± 0.2	0.8 ± 0.1	0.5 ± 0.1	0.2 ± 0.0
WZ	4.7 ± 0.6	1.4 ± 0.2	0.3 ± 0.0	0.1 ± 0.0
ZZ	0.1 ± 0.0	0.1 ± 0.0	0.0 ± 0.0	0.0 ± 0.0
Top	33.2 ± 5.7	100.3 ± 17.3	132.6 ± 22.8	51.4 ± 8.9
Z+jets	0.5 ± 0.2	0.5 ± 0.1	0.2 ± 0.0	0.0 ± 0.0
Zbb	1.5 ± 0.3	1.0 ± 0.2	0.3 ± 0.0	0.1 ± 0.0
Zcc	0.2 ± 0.0	0.2 ± 0.0	0.1 ± 0.0	0.0 ± 0.0
Wbb	83.4 ± 26.4	30.4 ± 9.6	7.9 ± 2.6	4.3 ± 1.4
Wcc/Wc	21.6 ± 6.8	9.8 ± 3.1	3.0 ± 1.0	1.9 ± 0.6
Total HF	104.9 ± 33.1	40.2 ± 12.6	10.9 ± 3.5	6.2 ± 2.0
Total MC	55.8 ± 8.2	111.8 ± 18.4	136.0 ± 23.1	52.3 ± 8.9
Mistags	21.9 ± 5.9	15.7 ± 3.8	8.9 ± 2.4	4.5 ± 1.3
Non-W	24.3 ± 9.7	24.3 ± 9.7	19.1 ± 7.7	0.0 ± 0.0
Total Prediction	206.9 ± 35.9	192.1 ± 24.6	174.9 ± 24.7	63.0 ± 9.2
Observed	180.0 ± 0.0	184.0 ± 0.0	186.0 ± 0.0	68.0 ± 0.0

Table 1: The number of expected single top and background events in 1.91fb^{-1} of CDF data passing all event selection for $W+2\text{b}$ -tagged jets.

This makes non-W fraction larger in anti-PHX estimation. As shown in Figure 4, anti-PHX estimation gives more than two times larger non-W fraction than jet-electron estimation. The anti-PHX template gives better agreement to data than jet-electron. To check this small W fraction in the anti-PHX template, we looked at W transverse mass and lepton eta times lepton charge. Figure 5 shows the W transverse mass distribution for each non-W template. There are no Jacobian peak around W mass. Lepton eta times lepton charge distributions are shown in Figure 6. $W+\text{jets}$ sample (top histograms) shows asymmetry since u or \bar{u} quarks in the proton or anti-proton have larger momentum than d or \bar{d} quarks. Though the anti-PHX template sample shows small asymmetry, the number of positive and negative events are consistent within the statistical uncertainty. These histograms conclude that W fraction in the anti-PHX template is small. We included the shape difference between anti-PHX and jet-electron as the systematic uncertainty.

2.5 effect of QCD cut removal and non-W modeling

We did not use QCD cut to increase the signal acceptance. If we apply the QCD cut, we lose 5.2 % of the s-channel single-top signal 2-jet-bin as shown in Table 3. We compared heavy flavor fraction and tagging efficiency between with and without QCD

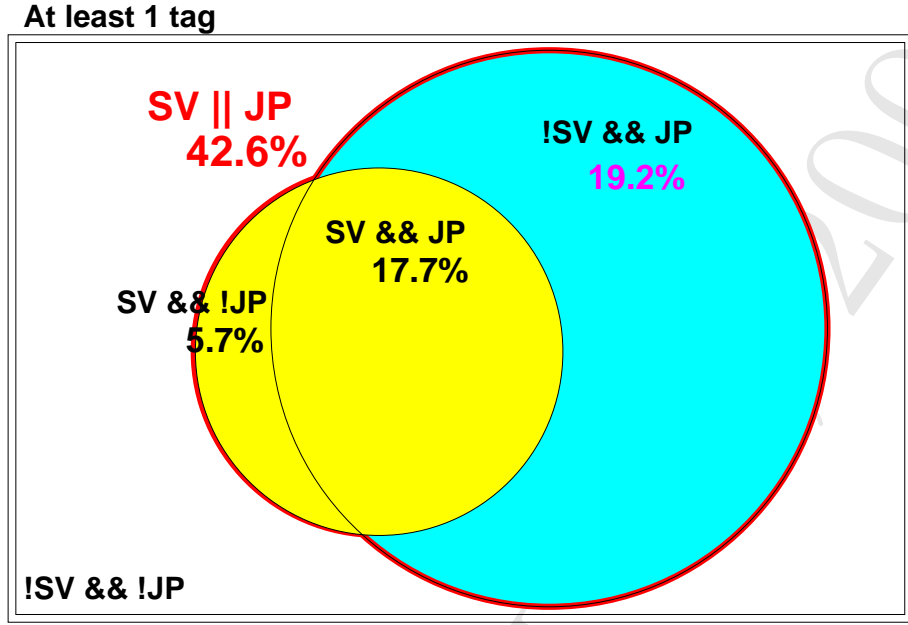


Figure 2: Second jet tagging efficiency for each categories. Yellow circle shows SecVtx double tag category. blue area shows one SecVtx tag and one JetProb tag excluding SecVtx double tag category.

variable	PHX
<i>ele->Region</i>	==plug
<i>ele->TrkZ0</i>	$\text{le } 60.0$
<i>ele->Et</i>	≥ 20
<i>ele->Pes2dEta</i>	$1.2 \leq \eta \leq 2.0$
<i>ele->HadEm</i>	≤ 0.05
<i>ele->PhxMatch</i>	true
<i>ele->TrkSiHits</i>	≥ 3
<i>ele->Pes2d5by9U</i>	≥ 0.65
<i>ele->Pes2d5by9V</i>	≥ 0.65
<i>ele->Pem3x3Chisq</i>	≤ 10
<i>ele->Pem3x3FitTow</i>	$\neq 0$
<i>ele->NumPes2d</i>	$\neq 0$
<i>ele->Isol</i>	$\text{le} 0.1$

Table 2: We choose red variables as the identification variables. The anti-PHX template was made using the event which passed all the kinematics variables(blue) but fails at least two identification(red) variables.

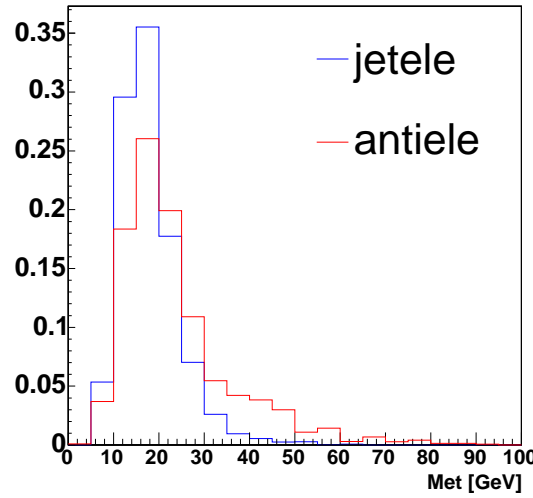


Figure 3: Shape comparison between anti-PHX and jet-electron. anti-PHX template have much more missing E_T than jet-electron template

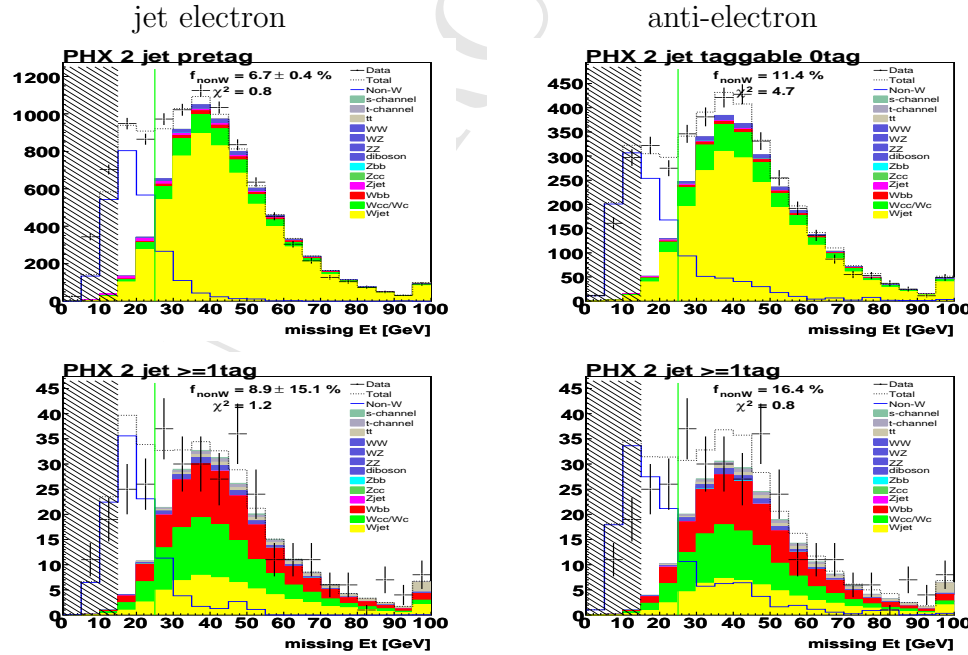
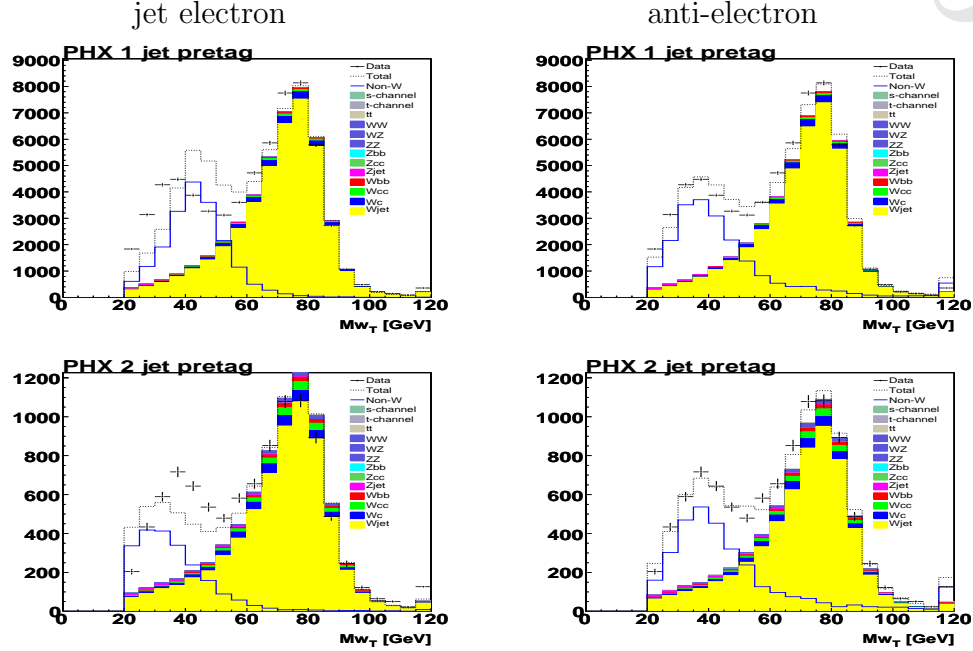
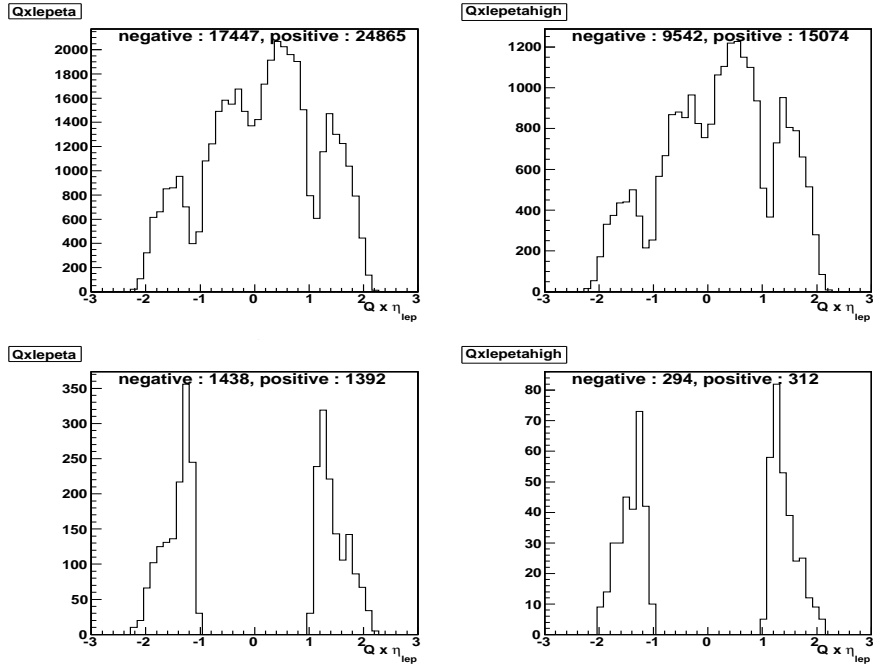


Figure 4: Non-W fit for pretag and at least one tag category. left hand side plots show anti-PHX and right hand side plots show jet-electron. We applied QCD veto for all histograms.

Figure 5: W transverse mass distribution for each templage.Figure 6: lepton charge times lepton eta distribution. upper histograms show $W+jets$ MC sample, and bottom histograms show anti-PHX template sample. left hand side shows all events, and right hand side shows high missing E_T (> 40 GeV) events

veto as listed in Table 5. All variables show good agreement within the error. We have the further merit for not using the QCD cut. It should make non-W systematics small since we could use more statistics for the non-W fitting. We measure the non-W fraction directly in the tagged sample. As the non-W template, we used the weighted anti-electron sample by mistag matrix. As the other background templates, we use our full background prediction with proper normalization except for non-W. Since we did not apply QCD veto, there are much more statistics than the template with QCD veto as shown in Table 4. In CEM, CMUP and CMX, the weighted anti-electron sample by mistag matrix is used as the non-W template. For the missing E_T fits in the PHX lepton category, we use anti-PHX sample as the non-W template [8]. To estimate the non-W fraction, we fitted the missing E_T distribution to a sum of background templates as shown in Figure 7-9 [7]. We included 40 % systematic uncertainty about non-W fit and non-W modeling. This value was used for the current all single top analyses in 1tag category. To check the difference of the uncertainty between 1tag and 2tag category, we considered the following two sources: First is the shape itself. We considered missing E_T threshold effect, changing the missing E_T threshold by ± 5 GeV. Second is the uncertainty on the missing E_T distribution due to the b-tagging. We estimated it as the difference between tagged template and weighted template using mistag matrix. Mistag matrix does not care about the missing E_T from b-jets, so the tagged sample has larger missing E_T than weighted sample as shown in figure 10. As the result, there is no difference between 1tag and 2tag category. Both of them are around 20%. Including the modeling uncertainty, we assigned 40 % on the uncertainty conservatively. Additionally we assigned 30 % systematic uncertainties for CEM pretag non-W fraction. Since the non-W modeling for the small missing E_T region does not look perfect. We evaluate this number with moving fit region.

	2jets	3jets
w/o !QCD	110671	34825
w/ !QCD	104916	32875
Efficiency	94.8%	94.4%

Table 3: The number of events which passed all event selection w/ and w/o QCD veto using stop00 pretag sample.

	CEM	PHX	CMUP	CMX
pretag	1638/26531	2223/30052	1362/22201	276/4330
≥ 1 tag	108/994	154/1494	89/842	19/152
SV+(SV JP)	13/108	12/152	10/93	3/15

Table 4: The number of remaining event($N_{antiele}^{E_T > 25\text{GeV}} / N_{antiele}^{tot}$) for non-W template sample.

with QCD cut

Heavy Flavor Fractions

	1Jet	2Jets	3Jets	4Jet	≥ 5 Jet
F_{HF}^{1b}	0.70	1.46	2.42	3.17	3.94
F_{HF}^{2b}	0.00	0.85	1.66	2.74	4.13
F_{HF}^{1c}	5.50	9.29	11.36	12.21	12.69
F_{HF}^{2c}	0.00	1.42	3.13	5.27	7.90

Tagging Efficiencies for at least 1 tag

	1Jet	2Jets	3Jets	4Jet	≥ 5 Jet
ϵ_{1b}	28.20	30.84	33.08	34.12	36.37
ϵ_{2b}	0.00	50.06	52.11	52.72	53.14
ϵ_{1c}	6.28	7.36	8.29	9.60	11.24
ϵ_{2c}	0.00	12.25	14.04	14.86	16.86

Tagging Efficiencies for at least 2 tag

	1Jet	2Jets	3Jets	4Jet	≥ 5 Jet
ϵ_{1b}	0.00	0.34	0.82	1.35	2.14
ϵ_{2b}	0.00	11.27	12.46	12.77	14.06
ϵ_{1c}	0.00	0.03	0.08	0.14	0.35
ϵ_{2c}	0.00	0.52	0.69	0.94	1.20

Tagging Efficiencies for SV+(JP&&!SV)

	1Jet	2Jets	3Jets	4Jet	≥ 5 Jet
ϵ_{1b}	0.00	1.19	2.71	4.32	5.68
ϵ_{2b}	0.00	8.83	10.52	11.89	12.86
ϵ_{1c}	0.00	0.21	0.54	1.04	1.59
ϵ_{2c}	0.00	1.45	2.03	2.55	3.60

without QCD cut

Heavy Flavor Fractions

	1Jet	2Jets	3Jets	4Jet	≥ 5 Jet
F_{HF}^{1b}	0.71	1.47	2.43	3.18	3.96
F_{HF}^{2b}	0.00	0.85	1.67	2.74	4.08
F_{HF}^{1c}	5.57	9.28	11.37	12.21	12.62
F_{HF}^{2c}	0.00	1.42	3.13	5.26	7.85

Tagging Efficiencies for at least 1 tag

	1Jet	2Jets	3Jets	4Jet	≥ 5 Jet
ϵ_{1b}	28.34	30.97	33.12	34.47	36.45
ϵ_{2b}	0.00	50.18	52.05	52.87	52.83
ϵ_{1c}	6.36	7.40	8.34	9.58	11.13
ϵ_{2c}	0.00	12.33	13.99	14.96	16.92

Tagging Efficiencies for at least 2 tag

	1Jet	2Jets	3Jets	4Jet	≥ 5 Jet
ϵ_{1b}	0.00	0.33	0.82	1.49	2.06
ϵ_{2b}	0.00	11.32	12.47	12.83	13.98
ϵ_{1c}	0.00	0.04	0.08	0.14	0.35
ϵ_{2c}	0.00	0.52	0.69	0.95	1.23

Tagging Efficiencies for SV+(JP&&!SV)

	1Jet	2Jets	3Jets	4Jet	≥ 5 Jet
ϵ_{1b}	0.00	1.21	2.76	4.37	5.64
ϵ_{2b}	0.00	8.89	10.63	11.90	12.99
ϵ_{1c}	0.00	0.21	0.54	1.03	1.56
ϵ_{2c}	0.00	1.49	2.01	2.56	3.64

Table 5: Heavy Flavor Fraction and Tagging Efficiency comparison.

3 S-channel Optimized Kinematic Fitter

There are two significant ambiguity in calculating the reconstructed M_{lnb} . One comes from the uncertainty on assigning a b-jet correctly to the b -jet from top quark decay. The other is the neutrino energy. Transverse energy of the neutrino can be measured indirectly as the missing transverse energy, but neutrino momentum z -component $P_z(\nu)$ can not be measured. The purpose of the kinematics fitter is to evaluate the neutrino momentum and find the right b-jet assignment.

3.1 Kinematics Fitter

Neutrino momentum z -component can be calculated as the solution in a quadratic equation using a W mass constraint and the missing transverse energy. Since we have two solutions at most, we constructed two types of likelihood-based kinematics fitter for 2 solutions case and the other case. We minimized the negative log likelihood value by varying three parameters, $P_Z(\nu Z)$, \not{E}_x and \not{E}_y . MINUIT was used this minimization.

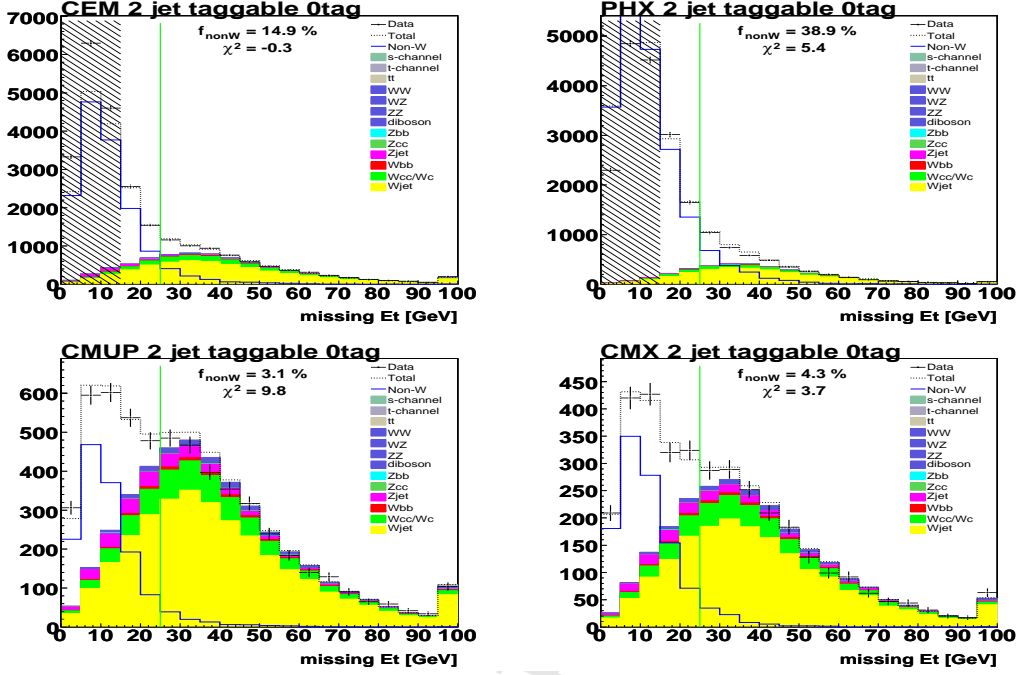


Figure 7: Non-W fit for pretag 2jet-bin.

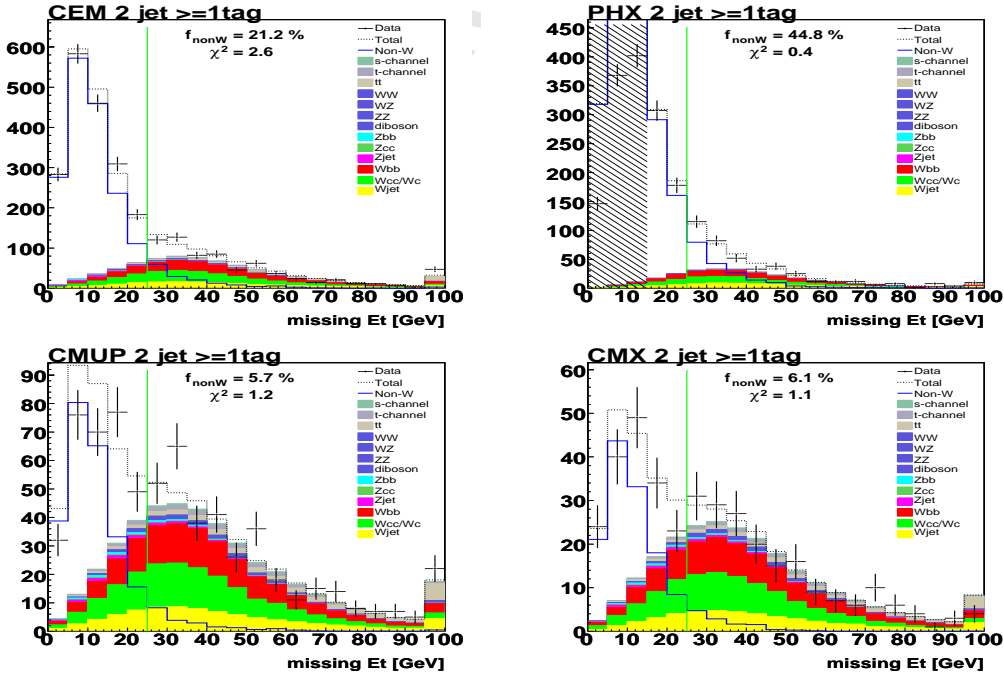


Figure 8: Non-W fit for at least 1 tag 2jet-bin.

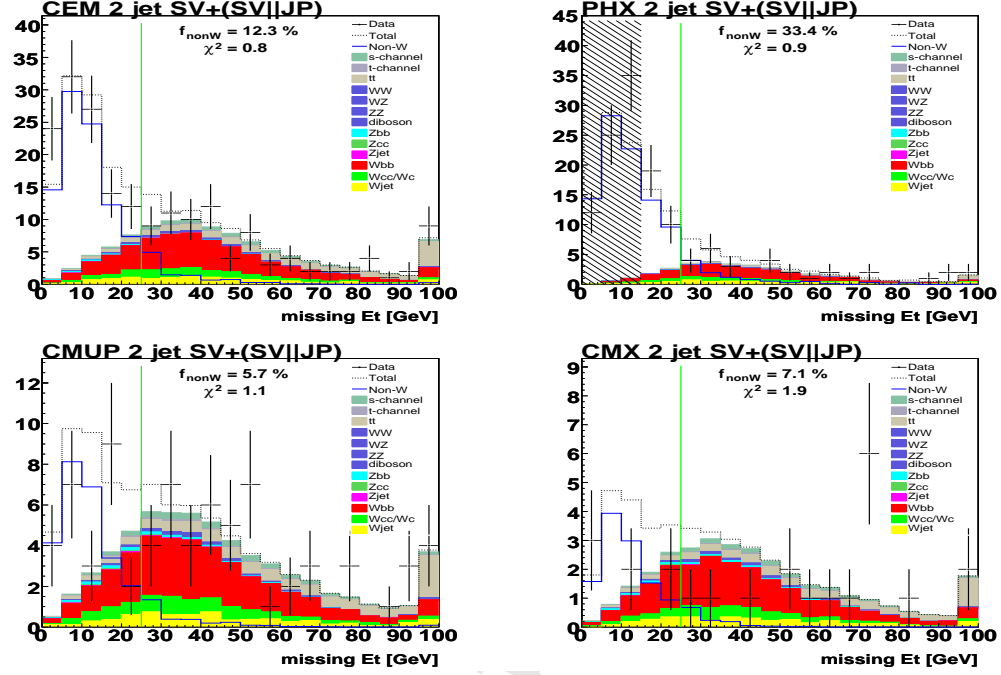


Figure 9: Non-W fit for SV+(SV||JP) 2jet-bin.

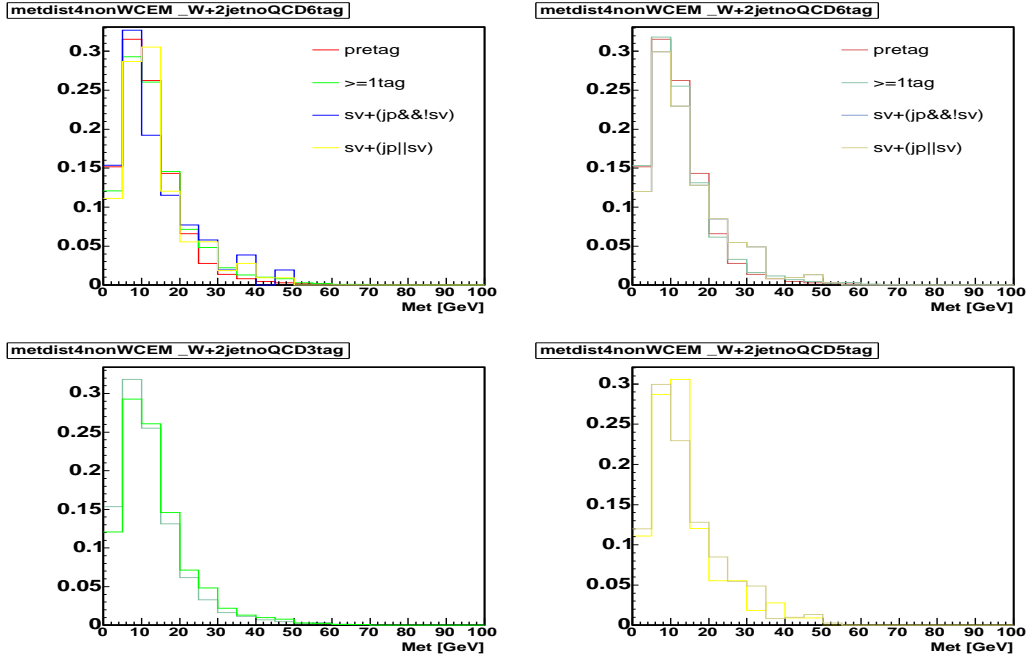


Figure 10: The caption.

We used the following likelihood : Two solutions case :

$$\mathcal{L}_{(P_{\nu Z}, \not{E}_x, \not{E}_y)} = \mathcal{L}_{P_{\nu Z}Q} \times \mathcal{L}_{M_{W^*}} \times \mathcal{L}_W \times \mathcal{L}_{\not{E}_x} \times \mathcal{L}_{\not{E}_y} \quad (1)$$

No (or one) solution case :

$$\mathcal{L}_{(P_{\nu Z}, \not{E}_x, \not{E}_y)} = \mathcal{L}_W \times \mathcal{L}_{\not{E}_x} \times \mathcal{L}_{\not{E}_y} \times \mathcal{L}_{sol} \quad (2)$$

where

$$\begin{aligned} \mathcal{L}_{P_{\nu Z}Q} &= \frac{P_{P_{\nu Z}Q}^{corr}}{P_{P_{\nu Z}Q}^{wrong}}, \quad \mathcal{L}_{M_{W^*}} = \frac{P_{M_{W^*}}^{corr}}{P_{M_{W^*}}^{wrong}}, \quad \mathcal{L}_W = \frac{1}{\Delta M_W^2 + \Gamma_W^2}, \quad -2 \log \mathcal{L}_{sol} = Im(Pz)^2 \\ \mathcal{L}_{\not{E}_x} &= \alpha \cdot e^{-\frac{(\Delta \not{E}_x)^2}{2\sigma_1^2}} + \beta \cdot e^{-\frac{(\Delta \not{E}_x)^2}{2\sigma_2^2}}, \quad \mathcal{L}_{\not{E}_y} = \alpha \cdot e^{-\frac{(\Delta \not{E}_y)^2}{2\sigma_1^2}} + \beta \cdot e^{-\frac{(\Delta \not{E}_y)^2}{2\sigma_2^2}} \end{aligned}$$

- $P_{\nu Z}Q - P_z^\nu$ solution times lepton charge
- M_{W^*} – invariant mass of all final particle.
- $W - W$ mass constraint.
- \not{E}_x – neutrino energy in x -direction.
- \not{E}_y – neutrino energy in y -direction.
- sol – Imaginaly part of the solution.

P_{val}^{corr} is a probability density function for the correct solution which is chosen it closer to hepg. P_{val}^{wrong} is a probability density function for the wrong solution.

Input template shapes were made with s-channel signal sample. Figure 11 shows the missing E_X and E_Y distributions. the $P_Z(\nu)$ solution times lepton charge distribution. Since u or \bar{u} quarks in the proton or anti-proton have larger momentum than d or \bar{d} quarks, W^* is boosted to the u type quark direction. This phenomena makes an asymmetry of this distribution. The correct solution which is just close to hepg $P_Z(\nu)$. Figure 11 also shows the reconstructed W^* mass distribution which is an invariant mass of all final particle.

As a result, reconstructed $P_Z(\nu)$ shows good agreement to the hepg $P_Z(\nu)$ as shown in Figure 12.

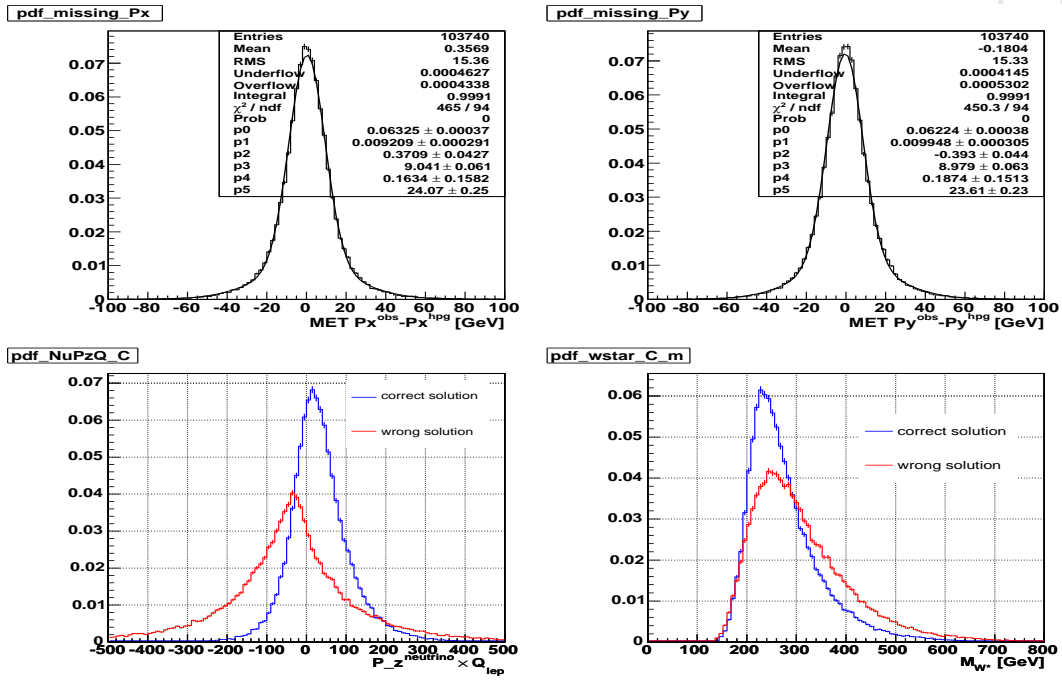


Figure 11: Missing Ex (top left) and Ey (top right) distribution. The Solid line showed best fit by double gaussian distribution. Neutrinino P_Z solution times lepton charge distribution (bottom left). Reconstructed mass distribution using all final particle. (bottom right). Blue line shows correct solution which is decided just close to hepg P_Z^ν . Red line shows wrong solution.

3.2 Likelihood for b-jet from top decay

In calculating kinematic variables for a single top search, one important decision is the choice of b-jet from top decay. In the 2-jet bin of the t-channel, this decision is relatively easy since 97 % of events have exactly one SECVTX tight tag in the at least one tag category. However in the 2-jet bin of the s-channel we have two real b-jets, so we could not use the b-tag information to choose the b-jet from top decay.

We construct a likelihood for b-jet from top decay as follows. $P_T(b)$, M_{lb} , $\cos\theta_b \times Q_{lep}$, where $P_T(b)$ is b-jet P_T , M_{lb} is an invariant mass of lepton + b-jet and $\cos\theta_b$, Q_{lep} is a scattering angle of b-jet in initial quarks ($q\bar{q}$) rest frame and Q_{lep} is a lepton charge. We pick up a b-jet which have larger likelihood as the b-jet from top decay.

$$\mathcal{L}_{bb} = \mathcal{L}_{bP_T} \times \mathcal{L}_{M_{lb}} \times \mathcal{L}_{\cos\theta_b \cdot Q_{lep}} \times \mathcal{L}_{M_{top}} \quad (3)$$

where

$$\mathcal{L}_{bP_T} = \frac{P_{P_T}^{b_{top}}}{P_{P_T}^{b_{other}}}, \quad \mathcal{L}_{M_{lb}} = \frac{P_{M_{lb}}^{b_{top}}}{P_{M_{lb}}^{b_{other}}}, \quad \mathcal{L}_{\cos\theta_b \cdot Q_{lep}} = \frac{P_{\cos\theta_b \cdot Q_{lep}}^{b_{top}}}{P_{\cos\theta_b \cdot Q_{lep}}^{b_{other}}}, \quad \mathcal{L}_{M_{top}} = \frac{1}{\Delta M_{M_{top}}^2 + \sigma_{M_{top}}^2}$$

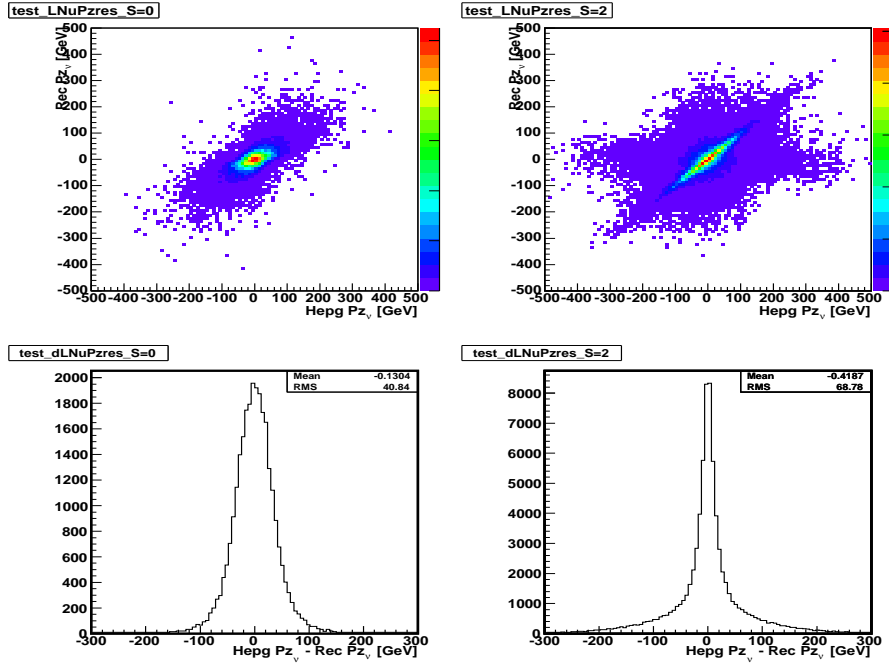


Figure 12: 2-demensional plot of the $P_Z(\nu)$ and hepg $P_Z(\nu)$. Left plots corresponds to show 0 or 1 solution case, and right plots to show 2 solutions case. Bottom histgrams show the pull distribution.

$P_{val}^{b_{top}}$ is a probability density function for the valiable using b-jet from top quark. $P_{val}^{b_{other}}$ is a probability density function for the valiable using the other b-jet.

Input template shapes were made with the s-channel single top signal sample. Figure 14 shows the b-jet transverse momentum distribution. The b-jet from top decay is more energetic than the other b-jet. The invariant mass distribution of lepton and b-jet and $\cos \theta_b$ times lepton charge distribution at initial two quarks($q\bar{q}'$) rest frame. Quarks are left-handed and anti-quarks are right-handed since s-channel process is completely weak interaction(V-A coupling). In Figure 13, blue arrows show the helicity direction of the particle. As we understand from this figure, it is easy for $b(\bar{b})$ quark coming from W^* to be produced in the direction of $P(\bar{P})$. This makes very larger difference in the $\cos \theta_b \times Q_{lep}$ distribution between b-jet from top decay and the other b-jet. As a result, This likelihood enables us to choose the b-jet from top decay with 82 % probability.

3.3 B-jet Energy Correction

The standard CDF jet energy corrections correct the energies of jets in a way that the mean of the corrected jet energies are set to the original parton energies for light flavor jets. The b-jets need further specific correction. So we obtained b-jet specific correction in the s-channel single top production process as shown in Figure 15.

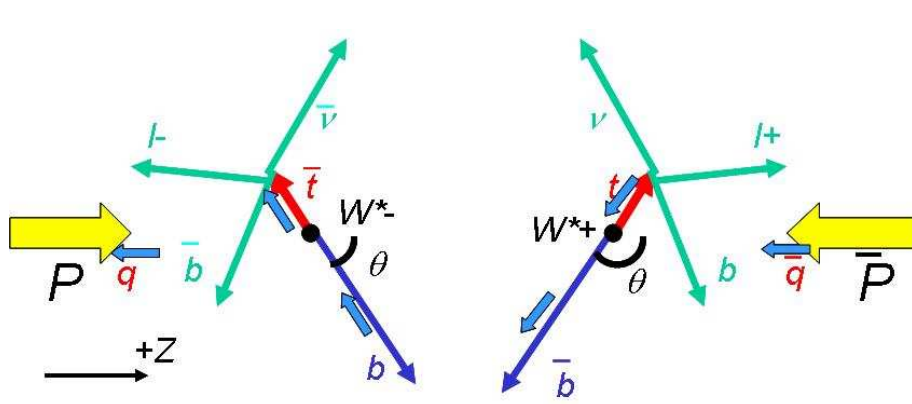
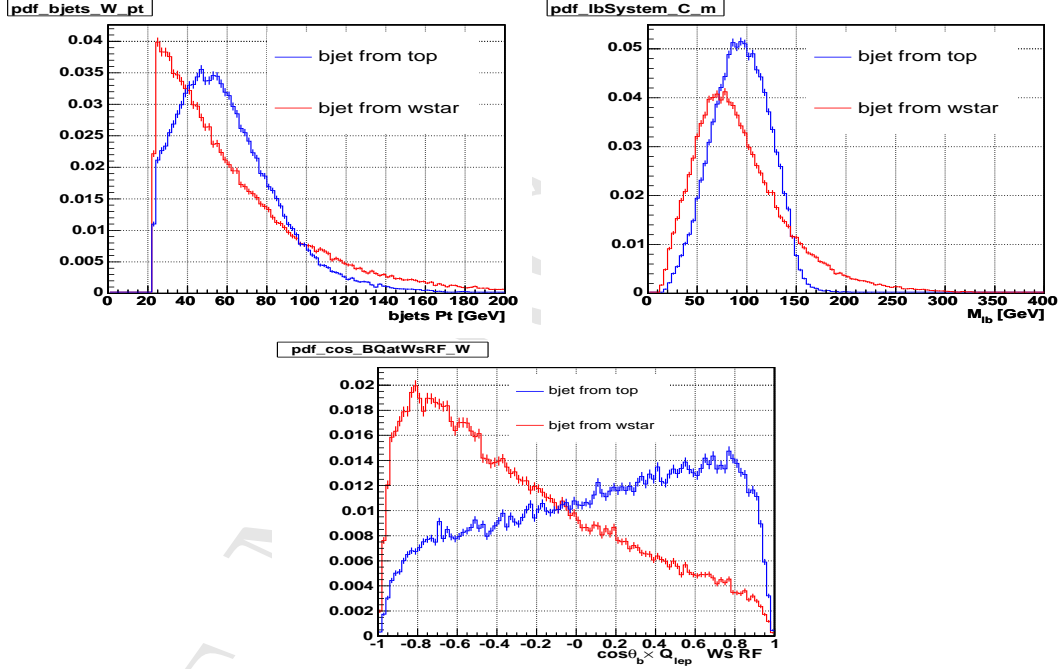
Figure 13: Final state behavior at the W^* rest frame

Figure 14: b-jet transverse momentum distribution (top left). Invariant mass distribution of lepton and b-jet (top right). cosine theta of b-jet times lepton charge distribution at initial two quarks($q\bar{q}'$) rest frame (bottom). Blue line histograms are made by using b-jet which is coming from top quark. Red line histograms are made by using the other b-jet.

Figure 16 shows the reconstructed top quark mass distribution. As a result, using the s-channel optimized kinematics fitter, top mass resolution is 24.5 GeV in r.m.s.

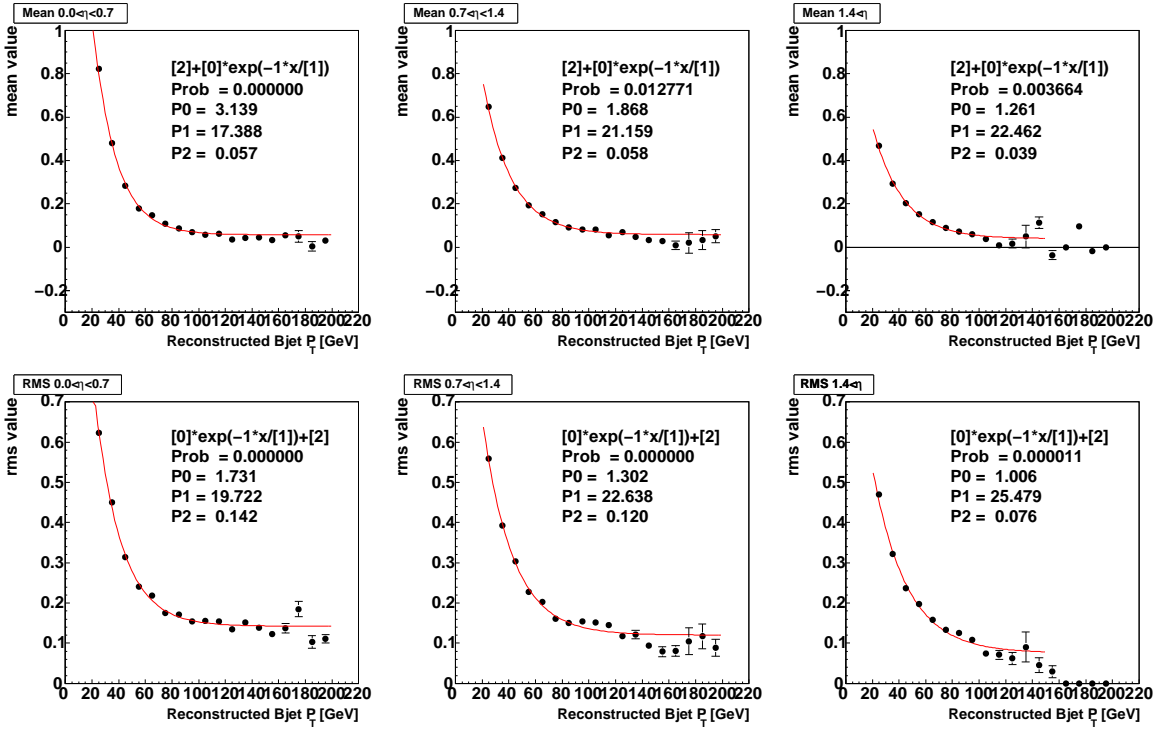


Figure 15: Top plots show the b-jet specific correction factor as a function of P_T . We divided it into three η range ($0 \leq |\eta| < 0.7$, $0.7 \leq |\eta| < 1.4$, $|\eta| \geq 1.4$). Bottom plots show the statistic uncertainties on the correction factor.

4 Likelihood-based separator of signal from background

In order to discover single top production, and to measure its rate with a highest precision, we must take advantage of as many differences between the signal and the background as possible. To this end, a variety of quantities which can be computed from the reconstructed event variables have been investigated for their ability to separate the signal from the background. No single variable encodes all conceivable separation, and so a likelihood is proposed to combine several variables together into one discriminant to compute the cross section limits or to discover the signal.

The Likelihood \mathcal{L} is constructed by first forming template histograms of each variable, separately for the signal and for the several background, denoted P_i^m for variable i for the background event class m and signal. Since about 75 % of the background are $W+HF$ and $t\bar{t}$, we used only $W+HF$ and $t\bar{t}$ for the background template as the first try. These two background classes are separately used to construct the likelihood.

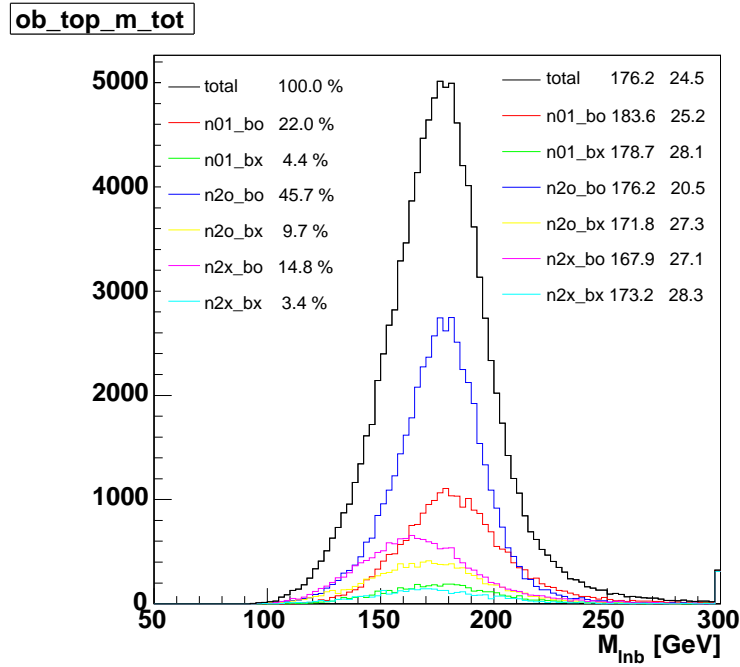


Figure 16: Black histogram shows reconstructed top mass distribution. Other color histograms show breakdown by using hepg information. The meaning of the legend are following. n01 is 0 or 1 solution. n2o is 2 solutions and correct solution. n2x is 2 solutions and wrong solution. bo is successful to choose b-jet combination. bx is failed to choose b-jet combination.

These histograms are normalized so that area is 1. The likelihood is defined as :

$$\mathcal{L}^{signal} = \frac{\prod_{i=1}^{n_{val}} P_i^{signal}}{\prod_{i=1}^{n_{val}} P_i^{signal} + \sum_{m=1}^{n_{bkg}} \prod_{i=1}^{n_{val}} P_i^m \times \alpha^m} \quad (4)$$

where,

$$P_i^{process} = \frac{f_i^{process}}{f_i^{signal} + \sum_{m=0}^{n_{bkg}} f_i^m}, \quad \alpha^m = \frac{N_{eve}^m}{\sum_{m=1}^{n_{bkg}} N_{eve}^m} \quad (5)$$

The likelihood ignores the correlation between the input variables, although it is critical that the predicted distributions of \mathcal{L} for the signal and the backgrounds are computed using a fully correlated set of input variables - from Monte Carlo or from control sample in the data as the correct modeling of the distribution of \mathcal{L} depends on the correct modeling of the correlations between the variables.

In order to obtain the likelihood we used the following six variables:

- M_{bb} : di-jet invariant mass
- Pt_{bb} : transverse momentum for bb system

- $M_{l\nu b}$: invariant mass of lepton, neutrino and b-jet from top quark
- $Pt(j1)$: leading jet transverse momentum
- Ht : transverse momentum scalar sum of lepton, neutrino and two jets
- \cancel{E}_T : Missing transverse energy
- $\mathcal{L}_{\nu\text{sol}} \times \mathcal{L}_{bb\text{sol}}$: kinematics fitter likelihood output times the likelihood for b-jet from top decay.

Figure 44 shows the input variables shape comparison between expected and observed. We included these plots for each double tag categories in appendix. The similar plots for our control region which event have two taggable jets but no tagged jet or one tagged jet is also included in appendix.

The distribution of likelihood separator is shown in Figure 19. We did some cross check for The output shape [9] for our two control samples and high score bins in the signal regions.

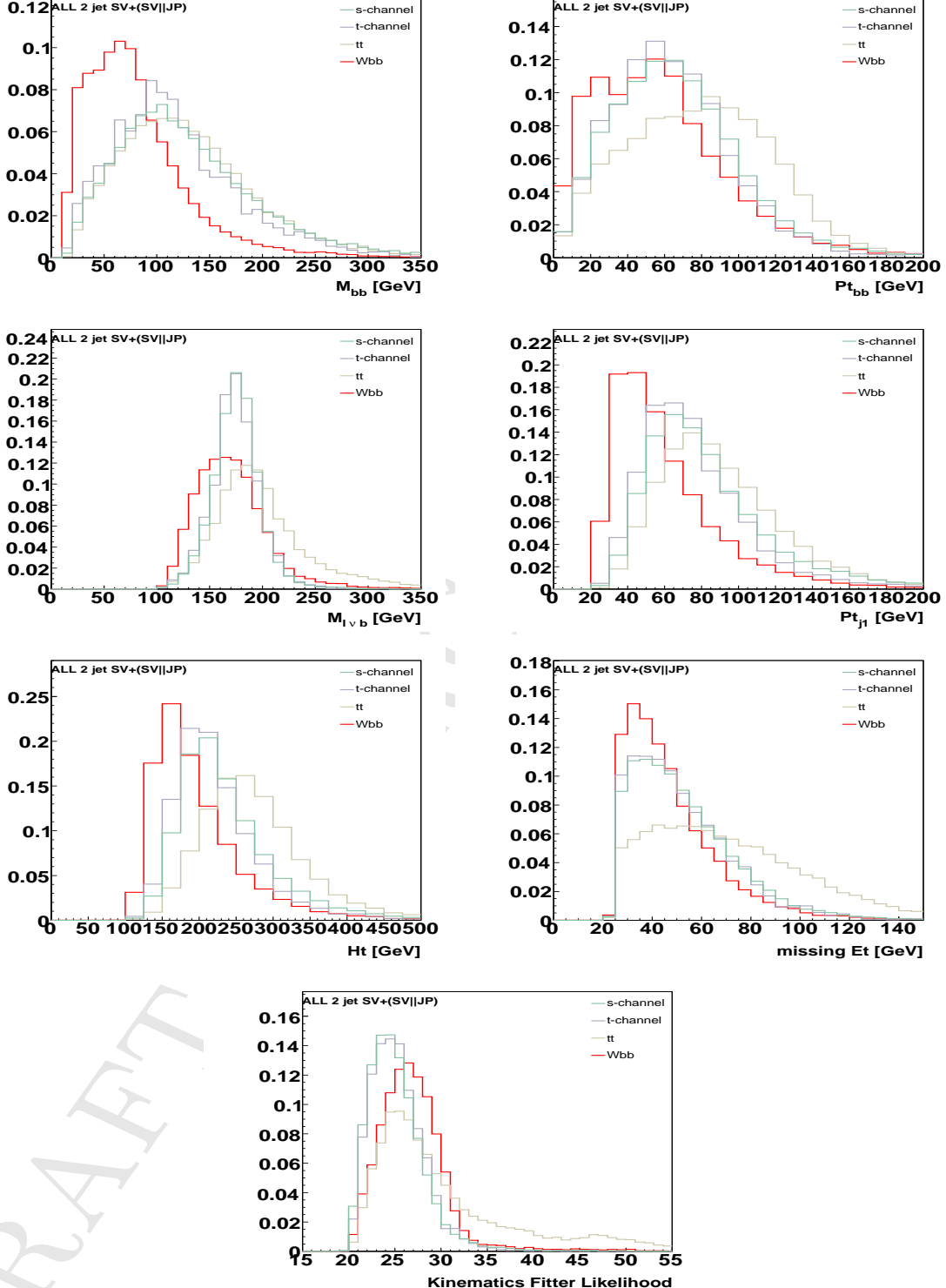


Figure 17: Input variables shape comparison for signal and main background (Wbb , $t\bar{t}$ and t-channel)

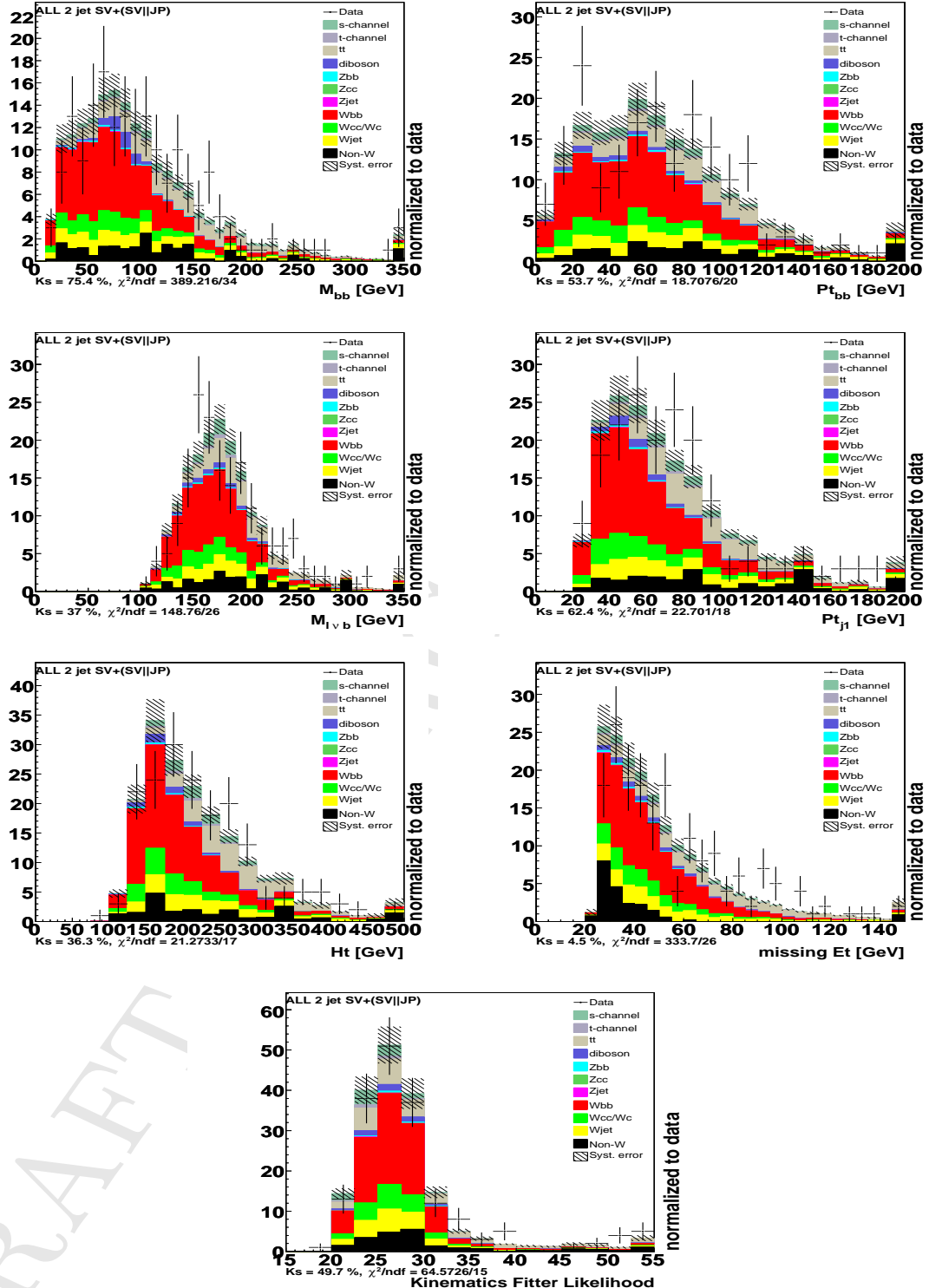


Figure 18: Input variables comparison between expected and observed. —

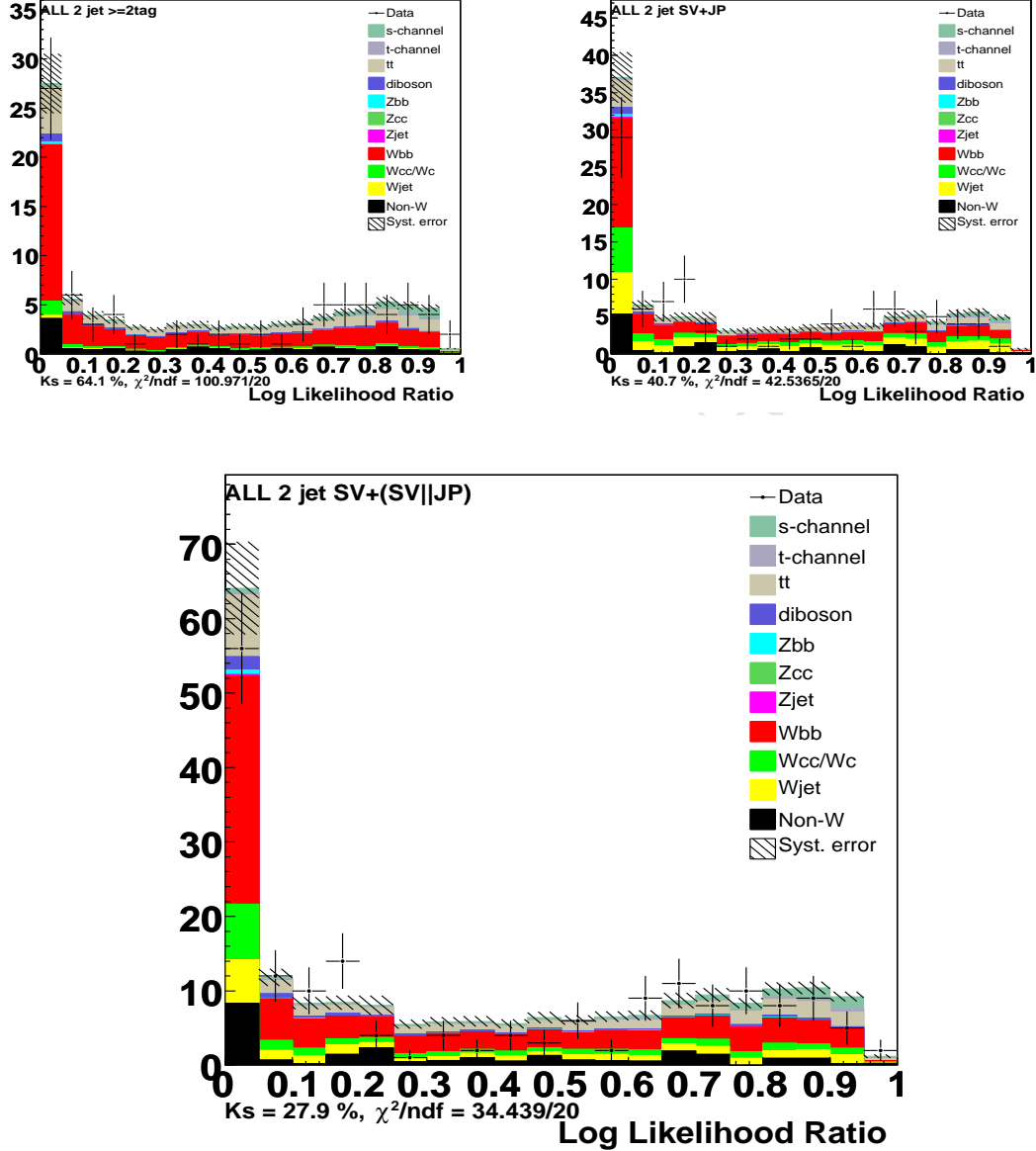


Figure 19: The likelihood output of signal and background separator for all double tag.

5 Systematic Uncertainties

The estimation of systematic uncertainties on the signal and background predictions are key ingredients in the procedure to search for single top production and the measurement of the cross section. As the systematic uncertainty, we consider uncertainties in the predicted rate of signal and background processes, and uncertainties in the shapes of the histogram templates.

Source	t -channel	s -channel	$t\bar{t}$	$Wc\bar{c}/Wc$	Wbb	$Z+jet$	Diboson
JES (+/-)	-3.6/3.5	-1.7/0.8	-7.9/8.5	4.1/-5.2	5.6/-6.2	1.4/-2.8	0.5/-2.8

Source	t -channel	s -channel	$t\bar{t}$
ISR less/more	-7.5/-0.1	-1.3/-4.5	-0.5/-7.6
FSR less/more	7.9/0.8	2.8/-1.6	-4.9/-1.1
PDF	not yet	not yet	not yet
MC generator	± 2.0	± 1.0	± 2.7
ϵ_{evt}	± 11.0	± 10.4	± 10.6
Luminosity	± 6.0	± 6.0	± 6.0
Cross section	± 12.6	± 12.4	± 12.4
M_{top} 172/178	4.4/-5.0	6.2/4.8	11.6/-10.3

Source	Diboson	$Z+jet$
ϵ_{evt}	± 10.8	± 14.7
Luminosity	± 6.0	± 6.0
Cross section	± 1.9	± 10.8

Source	mistag	non-W	wbb	wcc/wc
MethodII bkg estimation	± 24	± 40	± 31	± 31

Table 6: Fractional systematic rate uncertainties, in percent.

5.1 Rate Uncertainties

The predictions of the signal and background process rates have uncertainties from the method by which they are evaluated. For MC based backgrounds, Rate uncertainties are evaluated from source such as JES,ISR,FSR,PDF, event detection efficiency, theoretical cross section and the integrated luminosity estimation. In addition top mass uncertainty is also included for singletop and $t\bar{t}$ background. Tree-level Monte-Carlo predictions typically report corss sections that are low by K-factor which are process dependent, but usually are around 1.4. it have 30 % relative systematics uncertainty. Additional uncertainties arise from the flavor composition of various sample, particularly the $W+jets$ predictions. Non-W fraction has also systematic uncertainty described previous section. They are included as the Method II uncertainty. Table 6 detail the sources of rate uncertainty. it is also detailed in the singletop combination note [10].

5.2 Shape Uncertainties

The prediction of the template shape are also uncertain, due to deficiencies in the Monte Carlo samples, and the imperfection in the assumptions of using control sample distributions of data which are extrapolated to predict background in the signal sample. Since the entire histograms of the data in the selected signal region are used to extract cross section and significances, the shape uncertainties affect the resulting uncertainties of the results strongly. The background rates are constrained by the low signal-to-background portions of the discriminant histograms, and if the shapes are well known, these rates are easily converted into predictions in the high-score bins. But this is an extrapolation and shape uncertainties reduce our confidence in the predictions of the backgrounds in the high-score regions even though they are well known and modeled in the low score regions.

Some of the Monte Carlo based shape uncertainties can be estimated from prior guidelines for variation of the parameter of the prediction, such as ISR,FSR, M_T ,PDF and Q^2 uncertainties, while others arise from the observation of mismodeling of specific variables in the data.

Since the observed ΔR_{bb} and Pt_{bb} shapes for our control sample have the small excess, we also included the shape systematics for them.

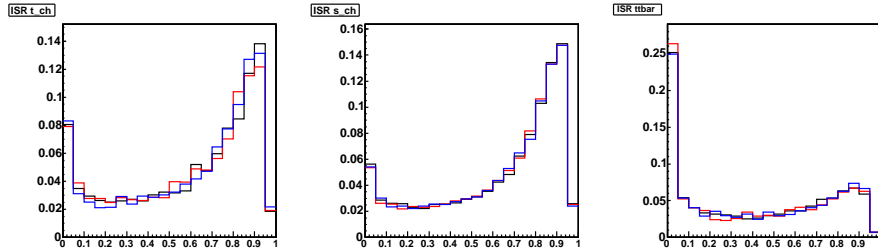


Figure 20: ISR shape uncertainty for t-channel(left), s-channel(middle) and $t\bar{t}$ (right).

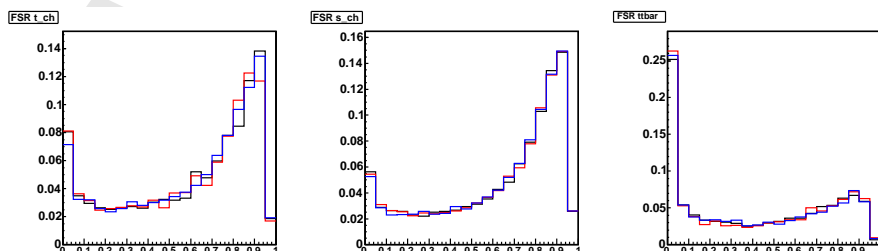


Figure 21: FSR shape uncertainty for t-channel(left), s-channel(middle) and $t\bar{t}$ (right).

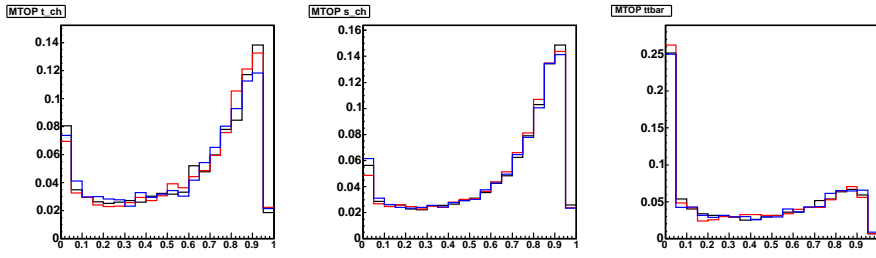


Figure 22: M_T shape uncertainty for t-channel(left), s-channel(middle) and $t\bar{t}$ (right).

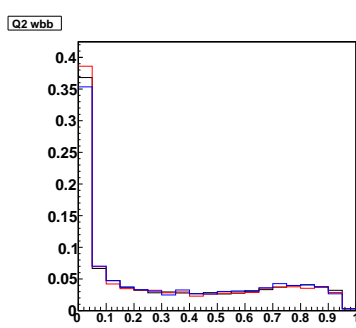


Figure 23: $AlpgenQ^2$ shape uncertainty for t-channel(left), s-channel(middle) and $t\bar{t}$ (right).

6 Expected Sensitivity and Hypothesis Test

We interpret the result using CLs/CLb method developed at LEP [11]. We compare our data against two models, one asserting that the data is due to background processes only (b) and one which includes StandardModel single top production in addition to the background processes (s+b). We propagate all systematic uncertainties in our statistical method. Using the test statistic $Q = \frac{\mathcal{L}(data|s+b)}{\mathcal{L}(data|b)}$ we compute the probability (p -value) that the background only model (b) fluctuated equal or up to the observed value Q_{obs} in the data (observed p value) and to the median Q value of signal+background (s+b) pseudo-experiment (expected p -value). Figure 25 shows the distribution of the test statistics for pseudo-experiments performed for (b) and (s+b). We expect a p -value of $\sim 0.21 \pm^{+0.37}_{-0.18} (1.25 \pm^{+0.89}_{-0.69} \sigma)$.

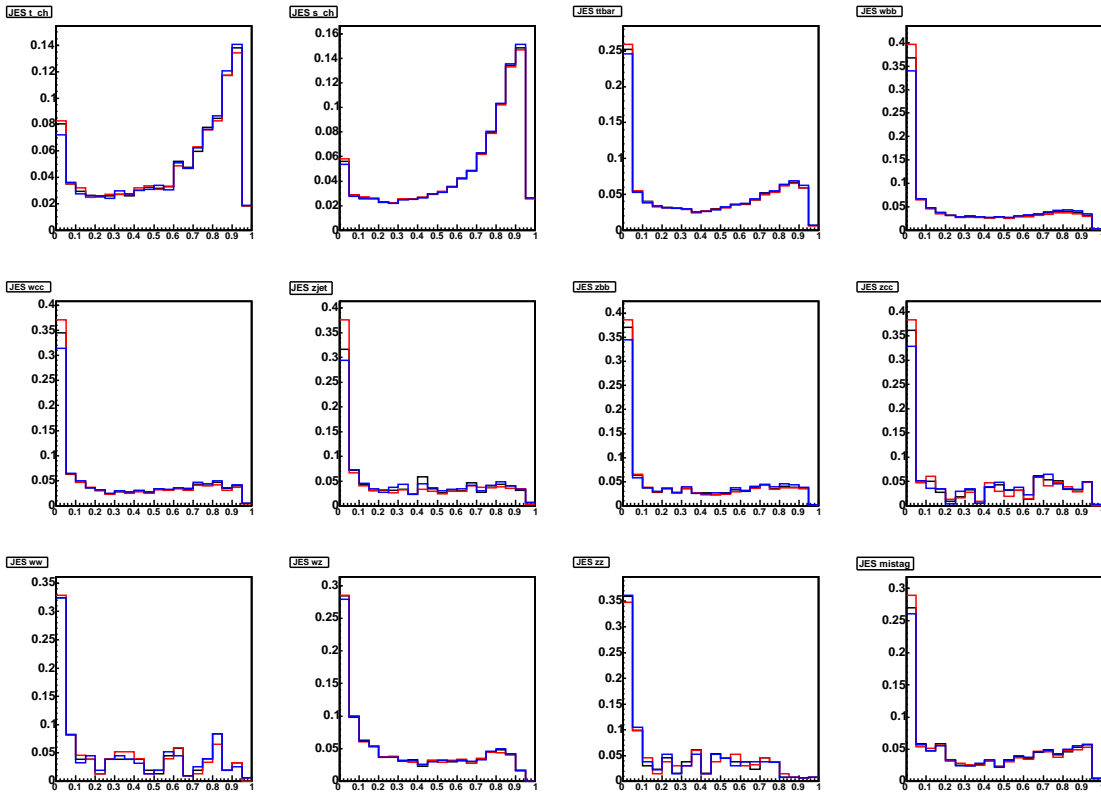


Figure 24: JES uncertainty.

7 Result with CDF II Data

As a result, no evidence is seen for single-top quark s-channel production as shown in Figure.25. There is 0.58σ excess over the Standard Model background. The 95 % CL. upper limit for the s-channel production cross section is set $\sigma_s = 2.35 \text{ pb}$ as shown in Figure.26.

8 Conclusions

We have searched s-channel electroweak single top quark production using double tag method with likelihood based signal background separator technique. We have analyzed 1.9 fb^{-1} of CDF Run II data and set the 95 % CL. single top s-channel cross section limit of :

$$\sigma_{\text{s-channel}}^{\text{obs}} = 2.35 \text{ pb} \quad (\sigma_{\text{s-channel}}^{\text{exp}} = 2.38 \text{ pb})$$

assuming a top quark mass of $175 \text{ GeV}/c^2$. The Observed p-value in 1.9 fb^{-1} of CDF data is $0.55\% (0.58\sigma)$. The expected p-value in pseudo-experiments is $\sim 0.21 \pm^{+0.37\%}_{-0.18\%} (1.25 \pm^{+0.89\%}_{-0.69\sigma})$.

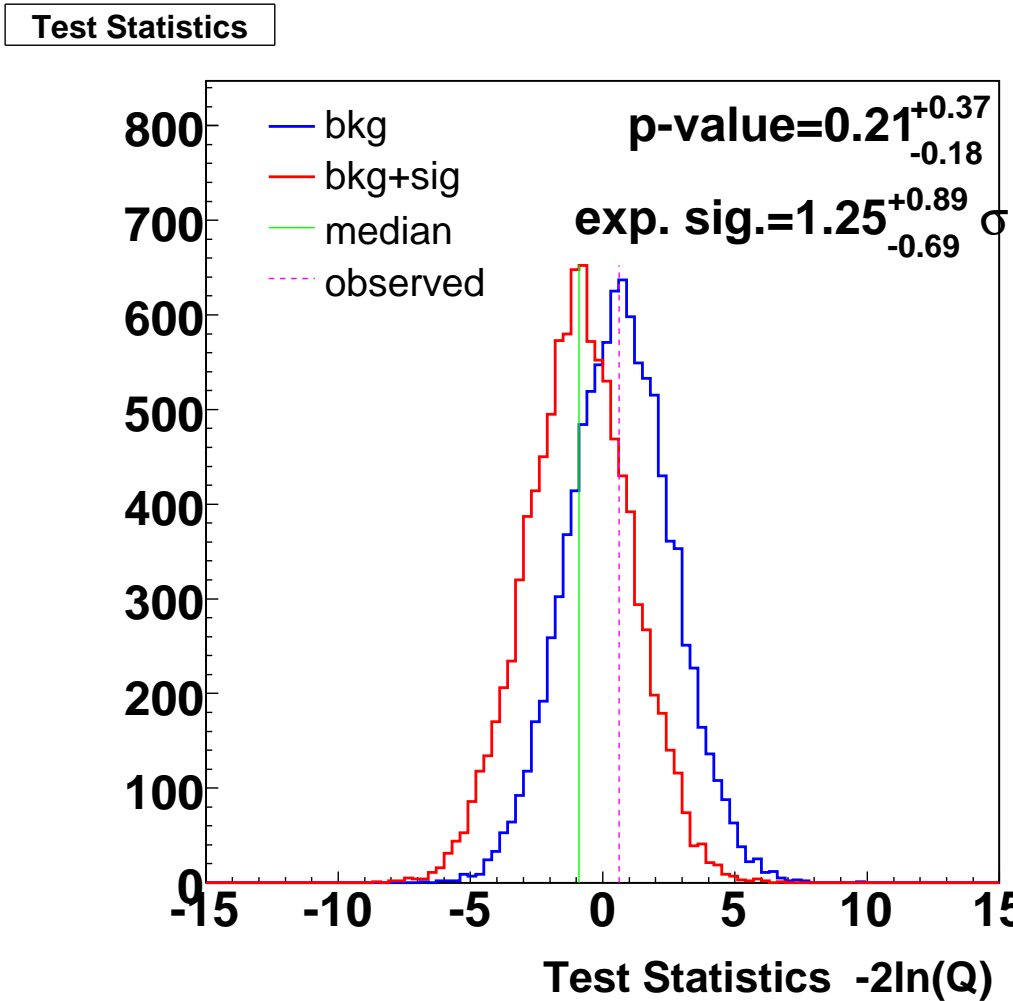


Figure 25: Distribution of the test statistics $Q = \frac{\mathcal{L}(\text{data}|s+b)}{\mathcal{L}(\text{data}|b)}$ for the single-top+background hypothesis and the background only hypothesis in 10000 pseudo-experiments. Left hand side is statistical uncertainty only calculation. Right hand side is included systematic uncertainties. The green line shows the median of the sig+bkg hypothesis which is used to determine the expected p -value.

Acknowledgments

Many thanks for a lot of people!

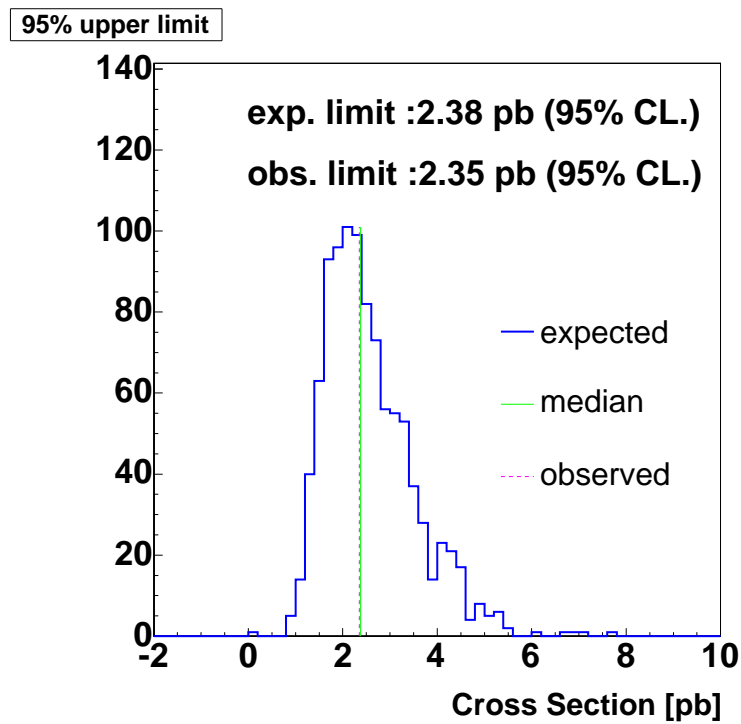


Figure 26: 95% CL. upper limit for the s-channel single top quark production cross section.

A Background Estimation table

≥ 2 SecVtx tag CEM Electrons				
Process	2jets	3jets	4jets	5jets
s-channel	3.5 ± 0.6	1.2 ± 0.2	0.3 ± 0.0	0.1 ± 0.0
t-channel	0.6 ± 0.1	0.9 ± 0.1	0.3 ± 0.0	0.1 ± 0.0
WW	0.1 ± 0.0	0.1 ± 0.0	0.0 ± 0.0	0.0 ± 0.0
WZ	1.2 ± 0.1	0.3 ± 0.0	0.1 ± 0.0	0.0 ± 0.0
ZZ	0.0 ± 0.0	0.0 ± 0.0	0.0 ± 0.0	0.0 ± 0.0
Top	9.3 ± 1.5	27.0 ± 4.3	36.6 ± 5.8	13.9 ± 2.2
Z+jets	0.0 ± 0.0	0.0 ± 0.0	0.0 ± 0.0	0.0 ± 0.0
Zbb	0.2 ± 0.0	0.2 ± 0.0	0.1 ± 0.0	0.0 ± 0.0
Zcc	0.0 ± 0.0	0.0 ± 0.0	0.0 ± 0.0	0.0 ± 0.0
Wbb	19.9 ± 6.3	7.1 ± 2.2	1.8 ± 0.6	1.0 ± 0.3
Wcc/Wc	1.9 ± 0.6	0.9 ± 0.3	0.3 ± 0.1	0.2 ± 0.1
Total HF	21.8 ± 6.9	8.0 ± 2.5	2.0 ± 0.7	1.2 ± 0.4
Total MC	14.8 ± 2.0	29.8 ± 4.5	37.3 ± 5.9	14.1 ± 2.2
Mistags	0.5 ± 0.4	0.4 ± 0.2	0.1 ± 0.1	0.1 ± 0.1
Non-W	5.6 ± 2.2	4.5 ± 1.8	3.8 ± 1.5	0.0 ± 0.0
Total Prediction	42.7 ± 7.5	42.7 ± 5.5	43.3 ± 6.1	15.3 ± 2.3
Observed	45.0 ± 0.0	51.0 ± 0.0	55.0 ± 0.0	20.0 ± 0.0

≥ 2 SecVtx PHX Electrons				
Process	2jets	3jets	4jets	5jets
s-channel	0.7 ± 0.1	0.2 ± 0.0	0.1 ± 0.0	0.0 ± 0.0
t-channel	0.2 ± 0.0	0.2 ± 0.0	0.1 ± 0.0	0.0 ± 0.0
WW	0.0 ± 0.0	0.0 ± 0.0	0.0 ± 0.0	0.0 ± 0.0
WZ	0.6 ± 0.1	0.1 ± 0.0	0.0 ± 0.0	0.0 ± 0.0
ZZ	0.0 ± 0.0	0.0 ± 0.0	0.0 ± 0.0	0.0 ± 0.0
Top	1.9 ± 0.3	5.6 ± 0.9	7.4 ± 1.2	2.8 ± 0.4
Z+jets	0.0 ± 0.0	0.0 ± 0.0	0.0 ± 0.0	0.0 ± 0.0
Zbb	0.1 ± 0.0	0.1 ± 0.0	0.0 ± 0.0	0.0 ± 0.0
Zcc	0.0 ± 0.0	0.0 ± 0.0	0.0 ± 0.0	0.0 ± 0.0
Wbb	7.3 ± 2.3	2.4 ± 0.8	0.4 ± 0.2	0.7 ± 0.2
Wcc/Wc	0.8 ± 0.3	0.3 ± 0.1	0.1 ± 0.0	0.2 ± 0.1
Total HF	8.2 ± 2.5	2.8 ± 0.9	0.4 ± 0.2	0.8 ± 0.3
Total MC	3.5 ± 0.4	6.3 ± 0.9	7.7 ± 1.2	2.8 ± 0.4
Mistags	0.3 ± 0.2	0.2 ± 0.1	0.0 ± 0.0	0.1 ± 0.1
Non-W	4.3 ± 1.7	7.0 ± 2.8	4.1 ± 1.6	0.0 ± 0.0
Total Prediction	16.2 ± 3.1	16.2 ± 3.1	12.2 ± 2.0	3.8 ± 0.5
Observed	13.0 ± 0.0	16.0 ± 0.0	13.0 ± 0.0	5.0 ± 0.0

≥ 2 SecVtx CMUP Muons

Process	2jets	3jets	4jets	5jets
s-channel	1.9 ± 0.3	0.7 ± 0.1	0.2 ± 0.0	0.0 ± 0.0
t-channel	0.3 ± 0.1	0.5 ± 0.1	0.2 ± 0.0	0.0 ± 0.0
WW	0.0 ± 0.0	0.0 ± 0.0	0.0 ± 0.0	0.0 ± 0.0
WZ	0.6 ± 0.1	0.2 ± 0.0	0.0 ± 0.0	0.0 ± 0.0
ZZ	0.0 ± 0.0	0.0 ± 0.0	0.0 ± 0.0	0.0 ± 0.0
Top	5.1 ± 0.8	15.3 ± 2.4	20.3 ± 3.2	7.7 ± 1.2
Z+jets	0.0 ± 0.0	0.0 ± 0.0	0.0 ± 0.0	0.0 ± 0.0
Zbb	0.3 ± 0.0	0.2 ± 0.0	0.0 ± 0.0	0.0 ± 0.0
Zcc	0.0 ± 0.0	0.0 ± 0.0	0.0 ± 0.0	0.0 ± 0.0
Wbb	11.6 ± 3.6	3.6 ± 1.1	1.1 ± 0.3	0.2 ± 0.1
Wcc/Wc	1.5 ± 0.4	0.5 ± 0.2	0.2 ± 0.1	0.0 ± 0.0
Total HF	13.1 ± 4.1	4.1 ± 1.3	1.3 ± 0.4	0.3 ± 0.1
Total MC	8.4 ± 1.1	16.9 ± 2.6	20.8 ± 3.3	7.8 ± 1.2
Mistags	0.3 ± 0.2	0.1 ± 0.1	0.1 ± 0.0	0.0 ± 0.0
Non-W	1.8 ± 0.7	1.8 ± 0.7	2.0 ± 0.8	0.0 ± 0.0
Total Prediction	23.5 ± 4.3	22.9 ± 2.9	24.1 ± 3.4	8.1 ± 1.2
Observed	21.0 ± 0.0	21.0 ± 0.0	20.0 ± 0.0	6.0 ± 0.0

 ≥ 2 SecVtx CMX Muons

Process	2jets	3jets	4jets	5jets
s-channel	0.9 ± 0.2	0.3 ± 0.1	0.1 ± 0.0	0.0 ± 0.0
t-channel	0.2 ± 0.0	0.3 ± 0.0	0.1 ± 0.0	0.0 ± 0.0
WW	0.0 ± 0.0	0.0 ± 0.0	0.0 ± 0.0	0.0 ± 0.0
WZ	0.4 ± 0.1	0.1 ± 0.0	0.0 ± 0.0	0.0 ± 0.0
ZZ	0.0 ± 0.0	0.0 ± 0.0	0.0 ± 0.0	0.0 ± 0.0
Top	2.6 ± 0.5	7.4 ± 1.3	9.9 ± 1.8	3.8 ± 0.7
Z+jets	0.0 ± 0.0	0.0 ± 0.0	0.0 ± 0.0	0.0 ± 0.0
Zbb	0.2 ± 0.0	0.1 ± 0.0	0.0 ± 0.0	0.0 ± 0.0
Zcc	0.0 ± 0.0	0.0 ± 0.0	0.0 ± 0.0	0.0 ± 0.0
Wbb	6.1 ± 1.9	2.1 ± 0.7	0.6 ± 0.2	0.2 ± 0.1
Wcc/Wc	0.5 ± 0.2	0.3 ± 0.1	0.1 ± 0.0	0.0 ± 0.0
Total HF	6.6 ± 2.1	2.4 ± 0.8	0.7 ± 0.2	0.2 ± 0.1
Total MC	4.3 ± 0.7	8.3 ± 1.4	10.2 ± 1.8	3.9 ± 0.7
Mistags	0.1 ± 0.1	0.1 ± 0.0	0.0 ± 0.0	0.0 ± 0.0
Non-W	0.3 ± 0.1	0.9 ± 0.3	1.3 ± 0.5	0.0 ± 0.0
Total Prediction	11.4 ± 2.2	11.6 ± 1.7	12.2 ± 1.9	4.1 ± 0.7
Observed	4.0 ± 0.0	7.0 ± 0.0	13.0 ± 0.0	6.0 ± 0.0

≥ 2 SecVtx All detectors

Process	2jets	3jets	4jets	5jets
s-channel	6.9 ± 1.1	2.4 ± 0.4	0.5 ± 0.1	0.1 ± 0.0
t-channel	1.3 ± 0.2	1.8 ± 0.3	0.6 ± 0.1	0.1 ± 0.0
WW	0.1 ± 0.0	0.1 ± 0.0	0.1 ± 0.0	0.0 ± 0.0
WZ	2.8 ± 0.3	0.8 ± 0.1	0.2 ± 0.0	0.0 ± 0.0
ZZ	0.1 ± 0.0	0.0 ± 0.0	0.0 ± 0.0	0.0 ± 0.0
Top	18.9 ± 3.0	55.4 ± 8.8	74.3 ± 11.8	28.3 ± 4.5
Z+jets	0.0 ± 0.0	0.1 ± 0.0	0.0 ± 0.0	0.0 ± 0.0
Zbb	0.8 ± 0.1	0.6 ± 0.1	0.1 ± 0.0	0.0 ± 0.0
Zcc	0.1 ± 0.0	0.0 ± 0.0	0.0 ± 0.0	0.0 ± 0.0
Wbb	44.9 ± 14.0	15.3 ± 4.7	3.8 ± 1.2	2.1 ± 0.6
Wcc/Wc	4.8 ± 1.5	2.1 ± 0.6	0.6 ± 0.2	0.5 ± 0.1
Total HF	49.7 ± 15.5	17.3 ± 5.4	4.5 ± 1.4	2.5 ± 0.8
Total MC	31.0 ± 4.1	61.2 ± 9.3	75.9 ± 12.0	28.7 ± 4.5
Mistags	1.2 ± 0.8	0.8 ± 0.4	0.3 ± 0.1	0.2 ± 0.1
Non-W	12.0 ± 4.8	14.1 ± 5.6	11.1 ± 4.5	0.0 ± 0.0
Total Prediction	93.8 ± 16.7	93.4 ± 12.1	91.8 ± 12.8	31.4 ± 4.6
Observed	83.0 ± 0.0	95.0 ± 0.0	101.0 ± 0.0	37.0 ± 0.0

SVJP CEM Electrons

Process	2jets	3jets	4jets	5jets
s-channel	2.3 ± 0.5	0.9 ± 0.2	0.2 ± 0.0	0.1 ± 0.0
t-channel	0.7 ± 0.1	0.8 ± 0.2	0.2 ± 0.0	0.0 ± 0.0
WW	0.5 ± 0.1	0.3 ± 0.1	0.1 ± 0.0	0.1 ± 0.0
WZ	0.9 ± 0.1	0.3 ± 0.0	0.1 ± 0.0	0.0 ± 0.0
ZZ	0.0 ± 0.0	0.0 ± 0.0	0.0 ± 0.0	0.0 ± 0.0
Top	7.1 ± 1.3	21.9 ± 4.2	28.7 ± 5.4	11.7 ± 2.2
Z+jets	0.2 ± 0.1	0.2 ± 0.0	0.1 ± 0.0	0.0 ± 0.0
Zbb	0.2 ± 0.0	0.2 ± 0.0	0.1 ± 0.0	0.0 ± 0.0
Zcc	0.0 ± 0.0	0.0 ± 0.0	0.0 ± 0.0	0.0 ± 0.0
Wbb	17.7 ± 5.8	6.7 ± 2.1	1.8 ± 0.6	1.0 ± 0.3
Wcc/Wc	7.3 ± 2.4	3.4 ± 1.1	1.1 ± 0.4	0.6 ± 0.2
Total HF	25.1 ± 8.1	10.1 ± 3.2	2.9 ± 1.0	1.6 ± 0.5
Total MC	11.9 ± 2.0	24.6 ± 4.5	29.5 ± 5.5	11.9 ± 2.3
Mistags	8.6 ± 2.3	7.4 ± 1.8	3.9 ± 1.3	2.1 ± 0.7
Non-W	5.4 ± 2.2	5.1 ± 2.0	3.5 ± 1.4	0.0 ± 0.0
Total Prediction	50.9 ± 8.9	47.1 ± 6.1	39.8 ± 5.9	15.7 ± 2.4
Observed	38.0 ± 0.0	42.0 ± 0.0	36.0 ± 0.0	18.0 ± 0.0

SVJP PHX Electrons

Process	2jets	3jets	4jets	5jets
s-channel	0.5 ± 0.1	0.2 ± 0.0	0.0 ± 0.0	0.0 ± 0.0
t-channel	0.2 ± 0.0	0.2 ± 0.0	0.0 ± 0.0	0.0 ± 0.0
WW	0.1 ± 0.0	0.1 ± 0.0	0.0 ± 0.0	0.0 ± 0.0
WZ	0.4 ± 0.1	0.1 ± 0.0	0.0 ± 0.0	0.0 ± 0.0
ZZ	0.0 ± 0.0	0.0 ± 0.0	0.0 ± 0.0	0.0 ± 0.0
Top	1.5 ± 0.3	4.5 ± 0.9	5.9 ± 1.1	2.3 ± 0.4
Z+jets	0.0 ± 0.0	0.0 ± 0.0	0.0 ± 0.0	0.0 ± 0.0
Zbb	0.1 ± 0.0	0.1 ± 0.0	0.0 ± 0.0	0.0 ± 0.0
Zcc	0.0 ± 0.0	0.0 ± 0.0	0.0 ± 0.0	0.0 ± 0.0
Wbb	6.2 ± 2.0	2.8 ± 0.9	0.4 ± 0.2	0.8 ± 0.2
Wcc/Wc	2.9 ± 0.9	1.3 ± 0.4	0.2 ± 0.1	0.6 ± 0.2
Total HF	9.0 ± 2.9	4.1 ± 1.3	0.6 ± 0.3	1.3 ± 0.4
Total MC	2.7 ± 0.4	5.2 ± 0.9	6.1 ± 1.1	2.4 ± 0.4
Mistags	4.4 ± 1.0	2.8 ± 0.7	0.7 ± 0.5	0.9 ± 0.3
Non-W	7.3 ± 2.9	7.2 ± 2.9	4.1 ± 1.6	0.0 ± 0.0
Total Prediction	23.5 ± 4.3	19.2 ± 3.4	11.5 ± 2.1	4.6 ± 0.7
Observed	17.0 ± 0.0	17.0 ± 0.0	10.0 ± 0.0	3.0 ± 0.0

SVJP CMUP Muons

Process	2jets	3jets	4jets	5jets
s-channel	1.3 ± 0.3	0.5 ± 0.1	0.1 ± 0.0	0.0 ± 0.0
t-channel	0.4 ± 0.1	0.4 ± 0.1	0.1 ± 0.0	0.0 ± 0.0
WW	0.3 ± 0.0	0.1 ± 0.0	0.1 ± 0.0	0.0 ± 0.0
WZ	0.4 ± 0.1	0.2 ± 0.0	0.0 ± 0.0	0.0 ± 0.0
ZZ	0.0 ± 0.0	0.0 ± 0.0	0.0 ± 0.0	0.0 ± 0.0
Top	3.9 ± 0.7	12.6 ± 2.4	15.9 ± 3.0	6.2 ± 1.2
Z+jets	0.2 ± 0.0	0.1 ± 0.0	0.0 ± 0.0	0.0 ± 0.0
Zbb	0.3 ± 0.1	0.2 ± 0.0	0.0 ± 0.0	0.0 ± 0.0
Zcc	0.1 ± 0.0	0.0 ± 0.0	0.0 ± 0.0	0.0 ± 0.0
Wbb	9.6 ± 3.1	3.7 ± 1.2	1.2 ± 0.4	0.3 ± 0.1
Wcc/Wc	4.3 ± 1.4	2.0 ± 0.6	0.7 ± 0.2	0.2 ± 0.1
Total HF	14.0 ± 4.4	5.7 ± 1.8	1.9 ± 0.6	0.4 ± 0.2
Total MC	6.9 ± 1.1	14.1 ± 2.6	16.4 ± 3.1	6.3 ± 1.2
Mistags	5.2 ± 1.2	3.3 ± 0.8	2.7 ± 0.8	0.8 ± 0.4
Non-W	1.6 ± 0.6	1.2 ± 0.5	3.3 ± 1.3	0.0 ± 0.0
Total Prediction	27.6 ± 4.8	24.4 ± 3.3	24.3 ± 3.5	7.5 ± 1.3
Observed	29.0 ± 0.0	24.0 ± 0.0	33.0 ± 0.0	7.0 ± 0.0

SVJP CMX Muons

Process	2jets	3jets	4jets	5jets
s-channel	0.6 ± 0.1	0.2 ± 0.0	0.1 ± 0.0	0.0 ± 0.0
t-channel	0.2 ± 0.0	0.2 ± 0.0	0.1 ± 0.0	0.0 ± 0.0
WW	0.1 ± 0.0	0.1 ± 0.0	0.0 ± 0.0	0.0 ± 0.0
WZ	0.2 ± 0.0	0.1 ± 0.0	0.0 ± 0.0	0.0 ± 0.0
ZZ	0.0 ± 0.0	0.0 ± 0.0	0.0 ± 0.0	0.0 ± 0.0
Top	1.9 ± 0.4	5.9 ± 1.2	7.9 ± 1.6	3.0 ± 0.6
Z+jets	0.1 ± 0.0	0.1 ± 0.0	0.0 ± 0.0	0.0 ± 0.0
Zbb	0.2 ± 0.0	0.1 ± 0.0	0.0 ± 0.0	0.0 ± 0.0
Zcc	0.0 ± 0.0	0.0 ± 0.0	0.0 ± 0.0	0.0 ± 0.0
Wbb	4.9 ± 1.6	1.9 ± 0.6	0.7 ± 0.2	0.2 ± 0.1
Wcc/Wc	2.2 ± 0.7	1.0 ± 0.3	0.4 ± 0.1	0.1 ± 0.0
Total HF	7.2 ± 2.3	3.0 ± 0.9	1.1 ± 0.3	0.3 ± 0.1
Total MC	3.4 ± 0.6	6.7 ± 1.4	8.1 ± 1.7	3.0 ± 0.6
Mistags	2.6 ± 0.8	1.5 ± 0.4	1.2 ± 0.3	0.5 ± 0.2
Non-W	1.2 ± 0.5	0.3 ± 0.1	1.1 ± 0.4	0.0 ± 0.0
Total Prediction	14.4 ± 2.6	11.5 ± 1.7	11.5 ± 1.8	3.8 ± 0.7
Observed	13.0 ± 0.0	6.0 ± 0.0	6.0 ± 0.0	3.0 ± 0.0

Process	SVJP All detectors			
	2jets	3jets	4jets	5jets
s-channel	4.7 ± 0.9	1.8 ± 0.3	0.4 ± 0.1	0.1 ± 0.0
t-channel	1.5 ± 0.3	1.6 ± 0.3	0.5 ± 0.1	0.1 ± 0.0
WW	1.0 ± 0.1	0.7 ± 0.1	0.3 ± 0.0	0.1 ± 0.0
WZ	1.9 ± 0.3	0.6 ± 0.1	0.1 ± 0.0	0.1 ± 0.0
ZZ	0.1 ± 0.0	0.0 ± 0.0	0.0 ± 0.0	0.0 ± 0.0
Top	14.3 ± 2.7	44.9 ± 8.5	58.4 ± 11.1	23.2 ± 4.4
Z+jets	0.5 ± 0.1	0.4 ± 0.1	0.1 ± 0.0	0.0 ± 0.0
Zbb	0.7 ± 0.1	0.5 ± 0.1	0.1 ± 0.0	0.0 ± 0.0
Zcc	0.1 ± 0.0	0.1 ± 0.0	0.0 ± 0.0	0.0 ± 0.0
Wbb	38.5 ± 12.4	15.2 ± 4.8	4.1 ± 1.3	2.2 ± 0.7
Wcc/Wc	16.8 ± 5.3	7.8 ± 2.4	2.3 ± 0.8	1.5 ± 0.5
Total HF	55.3 ± 17.7	22.9 ± 7.3	6.5 ± 2.1	3.7 ± 1.2
Total MC	24.8 ± 4.2	50.6 ± 9.2	60.1 ± 11.3	23.6 ± 4.5
Mistags	20.7 ± 5.1	14.9 ± 3.4	8.6 ± 2.3	4.3 ± 1.2
Non-W	15.6 ± 6.2	13.8 ± 5.5	12.0 ± 4.8	0.0 ± 0.0
Total Prediction	116.3 ± 19.8	102.3 ± 13.4	87.2 ± 12.7	31.6 ± 4.8
Observed	97.0 ± 0.0	89.0 ± 0.0	85.0 ± 0.0	31.0 ± 0.0

doubletag CEM Electrons

Process	2jets	3jets	4jets	5jets
s-channel	5.8 ± 1.0	2.1 ± 0.4	0.5 ± 0.1	0.1 ± 0.0
t-channel	1.3 ± 0.2	1.7 ± 0.3	0.5 ± 0.1	0.1 ± 0.0
WW	0.6 ± 0.1	0.4 ± 0.1	0.2 ± 0.0	0.1 ± 0.0
WZ	2.0 ± 0.3	0.6 ± 0.1	0.1 ± 0.0	0.0 ± 0.0
ZZ	0.0 ± 0.0	0.0 ± 0.0	0.0 ± 0.0	0.0 ± 0.0
Top	16.3 ± 2.8	48.9 ± 8.4	65.2 ± 11.2	25.6 ± 4.4
Z+jets	0.2 ± 0.1	0.2 ± 0.0	0.1 ± 0.0	0.0 ± 0.0
Zbb	0.4 ± 0.1	0.4 ± 0.1	0.1 ± 0.0	0.0 ± 0.0
Zcc	0.1 ± 0.0	0.1 ± 0.0	0.0 ± 0.0	0.0 ± 0.0
Wbb	37.6 ± 12.1	13.8 ± 4.3	3.6 ± 1.2	2.0 ± 0.7
Wcc/Wc	9.3 ± 3.0	4.3 ± 1.4	1.3 ± 0.5	0.8 ± 0.3
Total HF	46.9 ± 15.0	18.1 ± 5.7	4.9 ± 1.6	2.8 ± 0.9
Total MC	26.7 ± 3.9	54.4 ± 8.9	66.8 ± 11.3	26.0 ± 4.4
Mistags	9.1 ± 2.6	7.8 ± 2.0	4.0 ± 1.4	2.2 ± 0.7
Non-W	10.2 ± 4.1	8.2 ± 3.3	5.8 ± 2.3	0.0 ± 0.0
Total Prediction	92.9 ± 16.2	88.4 ± 11.3	81.5 ± 11.8	31.0 ± 4.6
Observed	83.0 ± 0.0	93.0 ± 0.0	91.0 ± 0.0	38.0 ± 0.0

doubletag PHX Electrons

Process	2jets	3jets	4jets	5jets
s-channel	1.1 ± 0.2	0.4 ± 0.1	0.1 ± 0.0	0.0 ± 0.0
t-channel	0.3 ± 0.1	0.4 ± 0.1	0.1 ± 0.0	0.0 ± 0.0
WW	0.1 ± 0.0	0.1 ± 0.0	0.1 ± 0.0	0.0 ± 0.0
WZ	1.0 ± 0.1	0.3 ± 0.0	0.1 ± 0.0	0.0 ± 0.0
ZZ	0.0 ± 0.0	0.0 ± 0.0	0.0 ± 0.0	0.0 ± 0.0
Top	3.4 ± 0.6	10.1 ± 1.7	13.3 ± 2.3	5.1 ± 0.9
Z+jets	0.0 ± 0.0	0.1 ± 0.0	0.0 ± 0.0	0.0 ± 0.0
Zbb	0.1 ± 0.0	0.1 ± 0.0	0.0 ± 0.0	0.0 ± 0.0
Zcc	0.0 ± 0.0	0.0 ± 0.0	0.0 ± 0.0	0.0 ± 0.0
Wbb	13.5 ± 4.2	5.2 ± 1.7	0.8 ± 0.4	1.4 ± 0.5
Wcc/Wc	3.7 ± 1.2	1.6 ± 0.5	0.3 ± 0.1	0.7 ± 0.2
Total HF	17.2 ± 5.4	6.8 ± 2.2	1.1 ± 0.5	2.2 ± 0.7
Total MC	6.2 ± 0.9	11.5 ± 1.9	13.8 ± 2.3	5.2 ± 0.9
Mistags	4.7 ± 1.2	2.9 ± 0.8	0.8 ± 0.6	1.0 ± 0.4
Non-W	10.0 ± 4.0	13.0 ± 5.2	8.0 ± 3.2	0.0 ± 0.0
Total Prediction	38.1 ± 6.9	34.2 ± 6.0	23.5 ± 4.0	8.4 ± 1.2
Observed	30.0 ± 0.0	33.0 ± 0.0	23.0 ± 0.0	8.0 ± 0.0

doubletag CMUP Muons

Process	2jets	3jets	4jets	5jets
s-channel	3.2 ± 0.6	1.1 ± 0.2	0.3 ± 0.1	0.1 ± 0.0
t-channel	0.7 ± 0.1	0.9 ± 0.2	0.3 ± 0.1	0.1 ± 0.0
WW	0.3 ± 0.0	0.2 ± 0.0	0.1 ± 0.0	0.0 ± 0.0
WZ	1.1 ± 0.1	0.3 ± 0.0	0.1 ± 0.0	0.0 ± 0.0
ZZ	0.1 ± 0.0	0.0 ± 0.0	0.0 ± 0.0	0.0 ± 0.0
Top	9.1 ± 1.6	28.0 ± 4.8	36.3 ± 6.2	13.9 ± 2.4
Z+jets	0.2 ± 0.0	0.1 ± 0.0	0.0 ± 0.0	0.0 ± 0.0
Zbb	0.6 ± 0.1	0.3 ± 0.1	0.1 ± 0.0	0.0 ± 0.0
Zcc	0.1 ± 0.0	0.1 ± 0.0	0.0 ± 0.0	0.0 ± 0.0
Wbb	21.2 ± 6.7	7.3 ± 2.3	2.3 ± 0.7	0.5 ± 0.2
Wcc/Wc	5.8 ± 1.8	2.5 ± 0.8	0.9 ± 0.3	0.2 ± 0.1
Total HF	27.0 ± 8.5	9.9 ± 3.1	3.1 ± 1.0	0.7 ± 0.3
Total MC	15.2 ± 2.2	31.0 ± 5.1	37.2 ± 6.3	14.1 ± 2.4
Mistags	5.4 ± 1.3	3.4 ± 0.9	2.8 ± 0.8	0.8 ± 0.4
Non-W	2.9 ± 1.1	2.3 ± 0.9	4.0 ± 1.6	0.0 ± 0.0
Total Prediction	50.6 ± 9.0	46.6 ± 6.1	47.1 ± 6.6	15.7 ± 2.5
Observed	50.0 ± 0.0	45.0 ± 0.0	53.0 ± 0.0	13.0 ± 0.0

doubletag CMX Muons

Process	2jets	3jets	4jets	5jets
s-channel	1.5 ± 0.3	0.6 ± 0.1	0.1 ± 0.0	0.0 ± 0.0
t-channel	0.4 ± 0.1	0.4 ± 0.1	0.1 ± 0.0	0.0 ± 0.0
WW	0.1 ± 0.0	0.1 ± 0.0	0.0 ± 0.0	0.0 ± 0.0
WZ	0.6 ± 0.1	0.2 ± 0.0	0.0 ± 0.0	0.0 ± 0.0
ZZ	0.0 ± 0.0	0.0 ± 0.0	0.0 ± 0.0	0.0 ± 0.0
Top	4.5 ± 0.9	13.3 ± 2.6	17.8 ± 3.4	6.8 ± 1.3
Z+jets	0.1 ± 0.0	0.1 ± 0.0	0.0 ± 0.0	0.0 ± 0.0
Zbb	0.4 ± 0.1	0.2 ± 0.0	0.1 ± 0.0	0.0 ± 0.0
Zcc	0.0 ± 0.0	0.0 ± 0.0	0.0 ± 0.0	0.0 ± 0.0
Wbb	11.0 ± 3.5	4.1 ± 1.3	1.3 ± 0.4	0.4 ± 0.1
Wcc/Wc	2.8 ± 0.9	1.3 ± 0.4	0.5 ± 0.2	0.2 ± 0.1
Total HF	13.8 ± 4.3	5.4 ± 1.7	1.8 ± 0.6	0.5 ± 0.2
Total MC	7.7 ± 1.3	15.0 ± 2.8	18.3 ± 3.5	6.9 ± 1.3
Mistags	2.7 ± 0.9	1.6 ± 0.4	1.3 ± 0.3	0.5 ± 0.2
Non-W	1.2 ± 0.5	0.9 ± 0.3	1.4 ± 0.6	0.0 ± 0.0
Total Prediction	25.4 ± 4.6	22.8 ± 3.3	22.8 ± 3.6	7.9 ± 1.3
Observed	17.0 ± 0.0	13.0 ± 0.0	19.0 ± 0.0	9.0 ± 0.0

doubletag All detectors

Process	2jets	3jets	4jets	5jets
s-channel	11.7 ± 2.0	4.2 ± 0.7	1.0 ± 0.2	0.2 ± 0.0
t-channel	2.7 ± 0.5	3.4 ± 0.6	1.0 ± 0.2	0.2 ± 0.0
WW	1.1 ± 0.2	0.8 ± 0.1	0.5 ± 0.1	0.2 ± 0.0
WZ	4.7 ± 0.6	1.4 ± 0.2	0.3 ± 0.0	0.1 ± 0.0
ZZ	0.1 ± 0.0	0.1 ± 0.0	0.0 ± 0.0	0.0 ± 0.0
Top	33.2 ± 5.7	100.3 ± 17.3	132.6 ± 22.8	51.4 ± 8.9
Z+jets	0.5 ± 0.2	0.5 ± 0.1	0.2 ± 0.0	0.0 ± 0.0
Zbb	1.5 ± 0.3	1.0 ± 0.2	0.3 ± 0.0	0.1 ± 0.0
Zcc	0.2 ± 0.0	0.2 ± 0.0	0.1 ± 0.0	0.0 ± 0.0
Wbb	83.4 ± 26.4	30.4 ± 9.6	7.9 ± 2.6	4.3 ± 1.4
Wcc/Wc	21.6 ± 6.8	9.8 ± 3.1	3.0 ± 1.0	1.9 ± 0.6
Total HF	104.9 ± 33.1	40.2 ± 12.6	10.9 ± 3.5	6.2 ± 2.0
Total MC	55.8 ± 8.2	111.8 ± 18.4	136.0 ± 23.1	52.3 ± 8.9
Mistags	21.9 ± 5.9	15.7 ± 3.8	8.9 ± 2.4	4.5 ± 1.3
Non-W	24.3 ± 9.7	24.3 ± 9.7	19.1 ± 7.7	0.0 ± 0.0
Total Prediction	206.9 ± 35.9	192.1 ± 24.6	174.9 ± 24.7	63.0 ± 9.2
Observed	180.0 ± 0.0	184.0 ± 0.0	186.0 ± 0.0	68.0 ± 0.0

B input variables

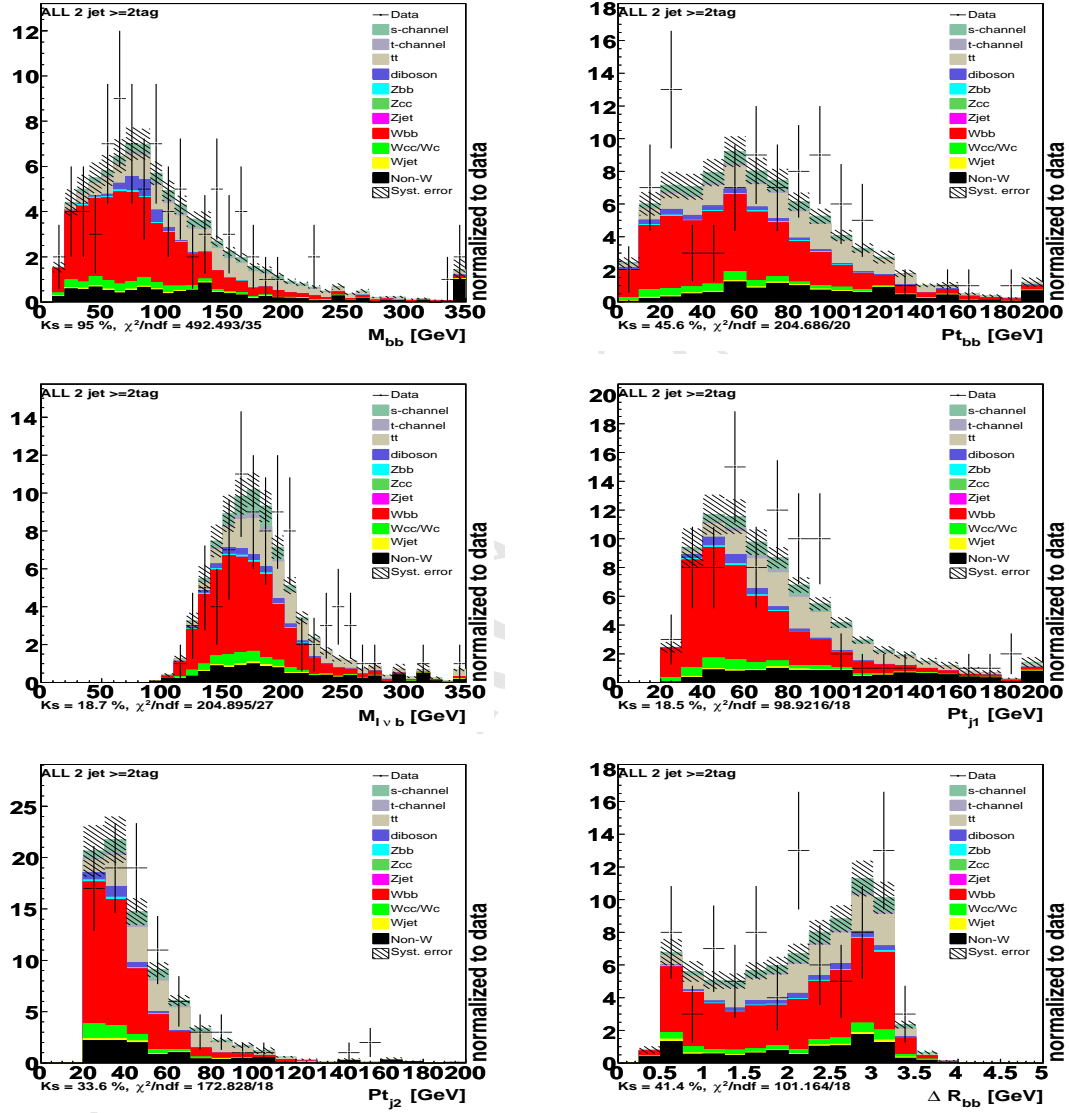


Figure 27: Input variables comparison between expected and observed. – SV + SV.

References

- [1] CDF Single Top Group *Search for single top-quark production with neural networks using 1.9 fb⁻¹* CDF 9107 (2007)

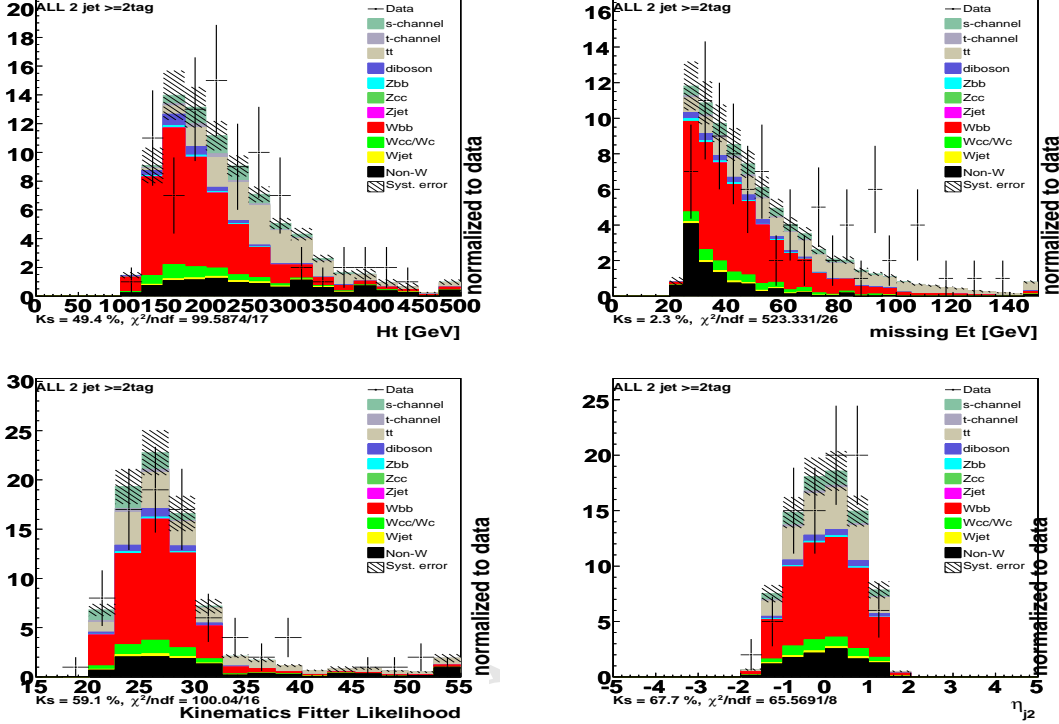


Figure 28: Input variables comparison between expected and observed. – SV + SV.

- [2] CDF Single Top Group *Likelihood Function Search for Sintle-top Production with 1.9 fb^{-1} of Data* CDF 9112 (2007)
- [3] CDF Single Top Group *Search for Single Top Quark Production using the Matrix Element Technique* CDF 9117 (2007)
- [4] CDF Single Top Group *Event detection efficiency for single-top evets and MC based background estimate for Summer 2006*, CDF 8286 (2006)
- [5] CDF Single Top Group *Data based background estimate for Summer 2006*, CDF 8292 (2006)
- [6] J.Adelman et al. *Method II for you*, CDF 9185 (2008)
- [7] CDF Single Top Group *Estimation and modeling of non-W background for single-top searches*, CDF 8489 (2006)
- [8] Jay Dittmann et al. *Search for Higgs Boson Production in Association with W Boson with 1.9 fb^{-1}* , CDF 9136 (2008)
- [9] <http://www-cdf.fnal.gov/kojin/internal/singletop/gen6/QandA/>, Q & A web page for 1.9 fb^{-1} .

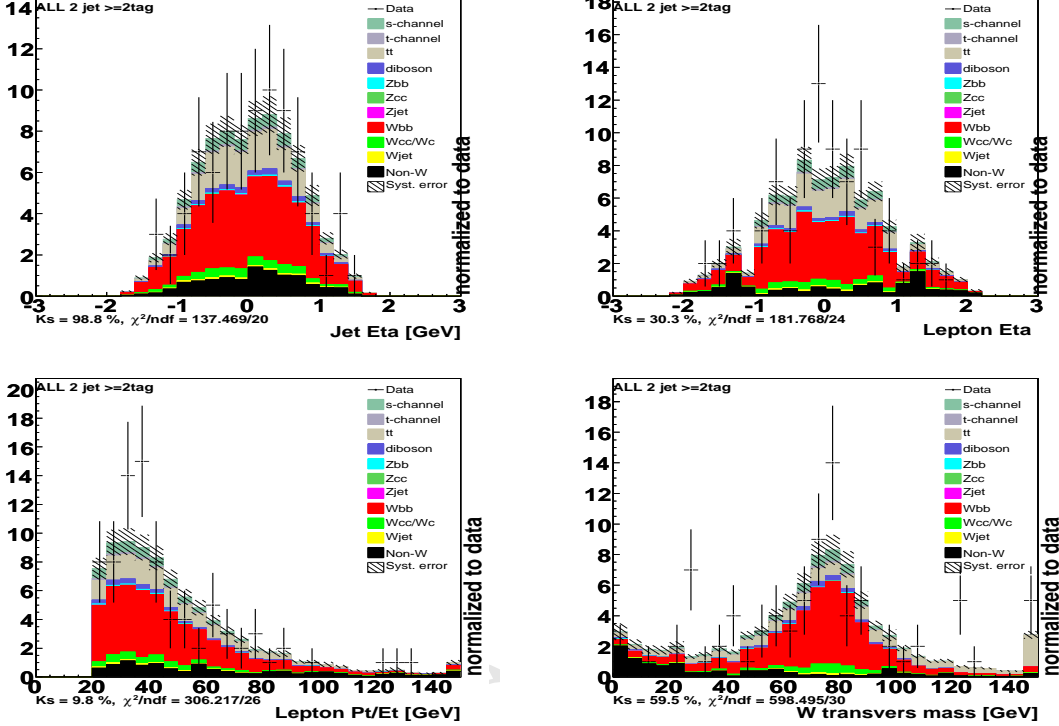


Figure 29: Input variables comparison between expected and observed. – SV + SV.

- [10] CDF Single Top Group *Combination of the Single-Top Results with 2fb⁻¹*, CDF 9173 (2008)
- [11] L. Read, J.Phys G 28, 2693 (2002) and T.Junk, Nucl.Instrum. Meth. 434,435(1999). See also P.Bock et al. (The LEP Collaborations), CERN-EP-98-046(1998) and CERN-EP-2000-055(2000). 3 3 3 4 4 4 9 9 19 23 25

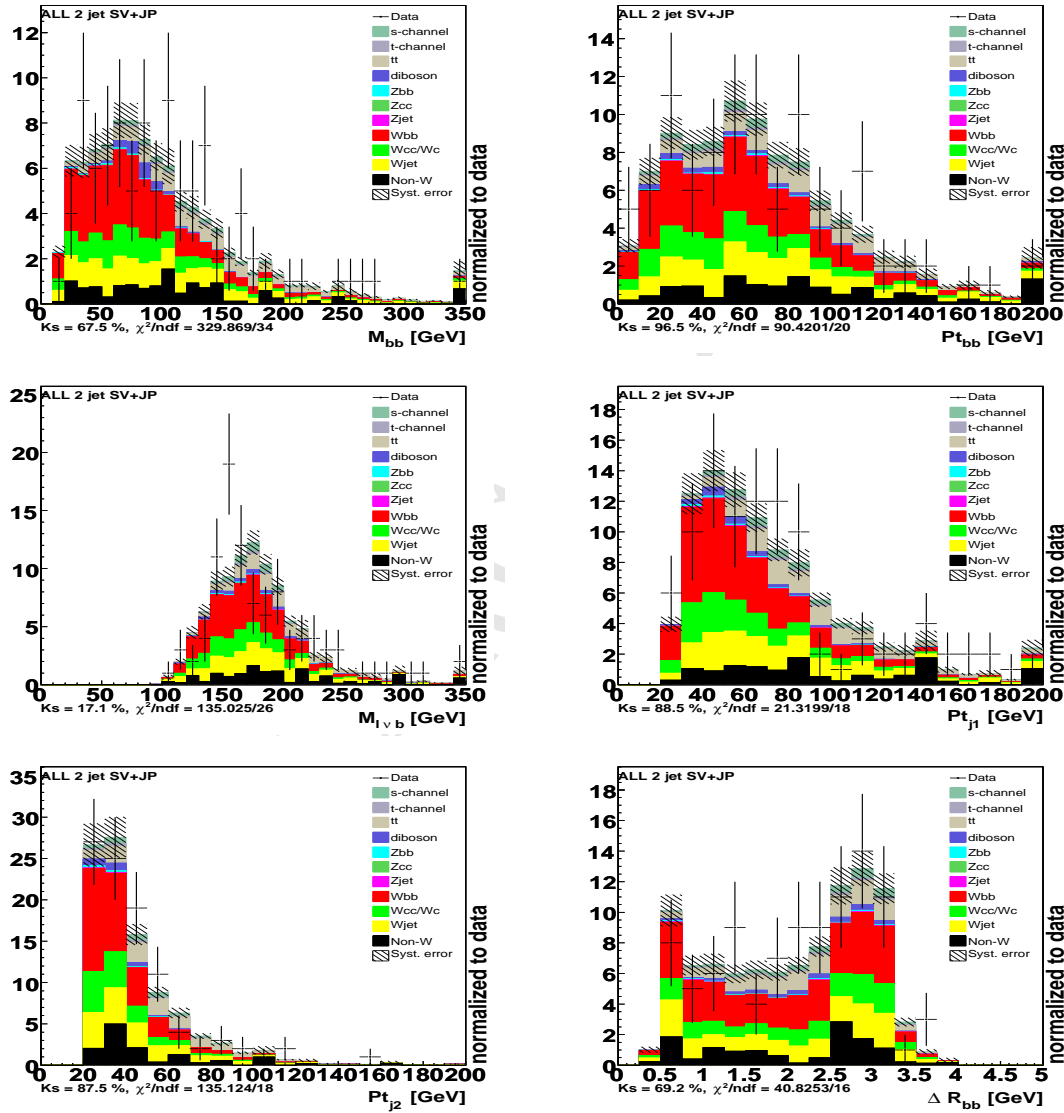


Figure 30: Input variables comparison between expected and observed. – SV + (JP&&!SV).

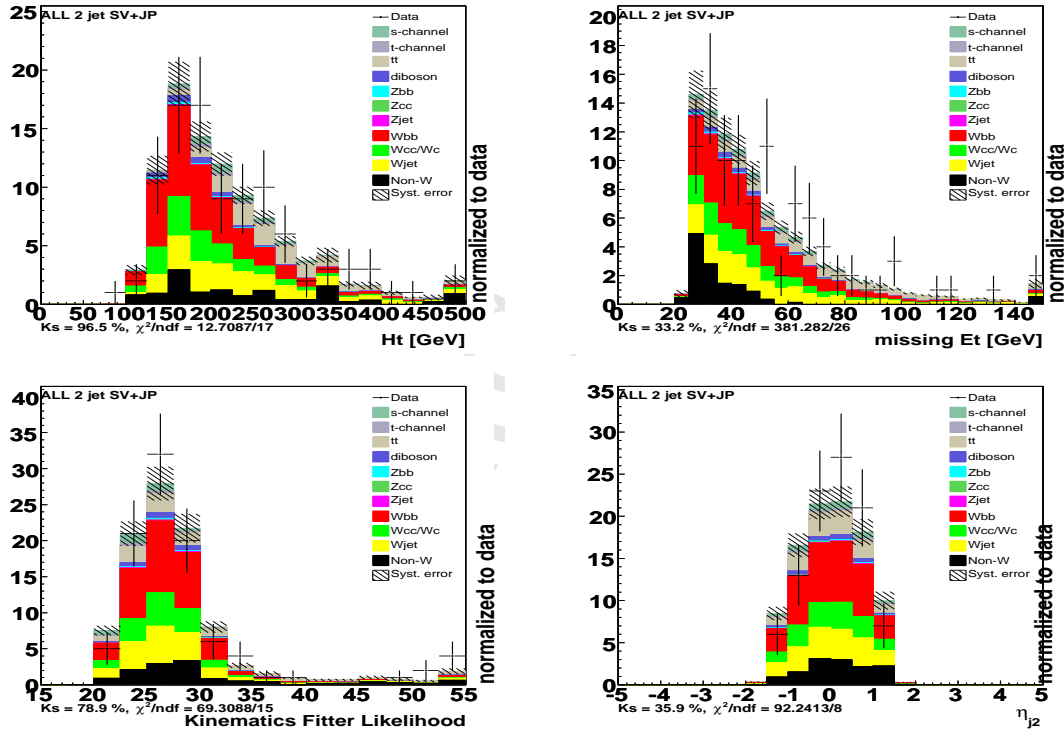


Figure 31: Input variables comparison between expected and observed. – SV + (JP&&!SV).

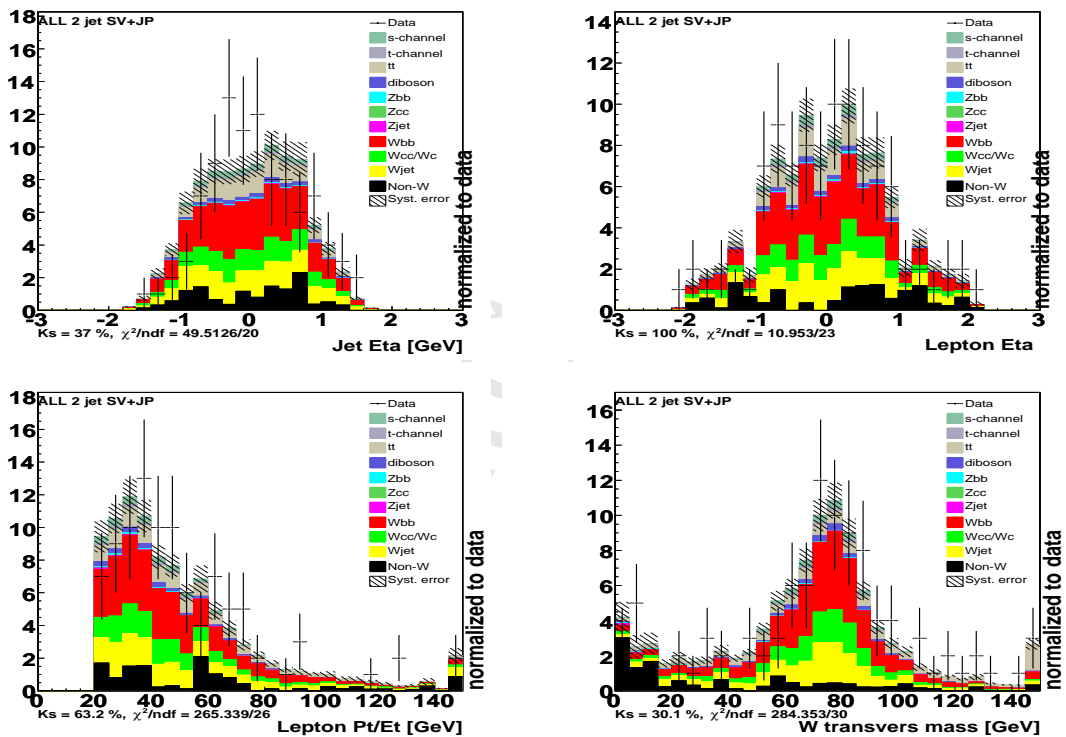


Figure 32: Input variables comparison between expected and observed. – SV + (JP&&!SV).

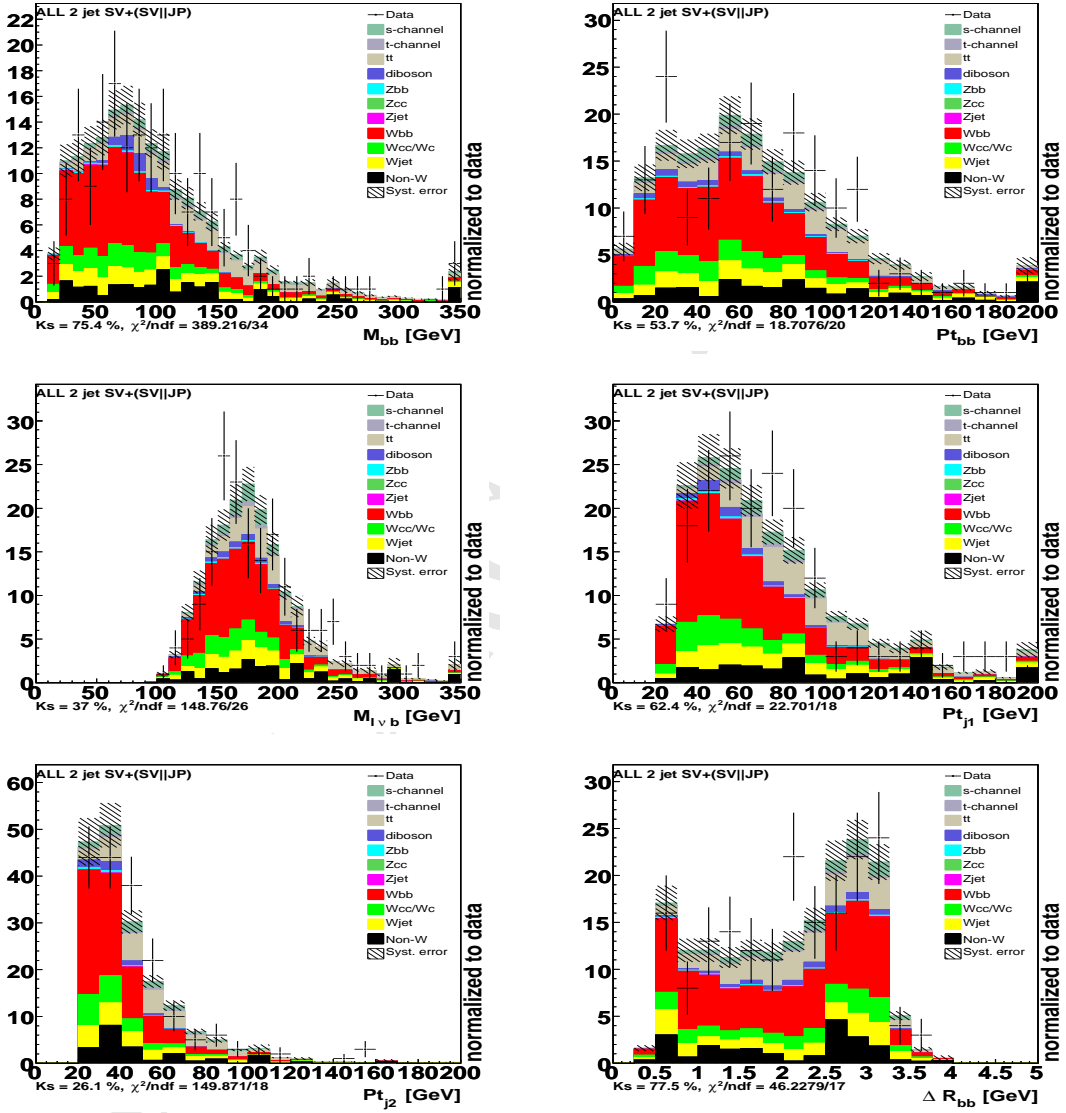


Figure 33: Input variables comparison between expected and observed. – SV + (JP||SV).

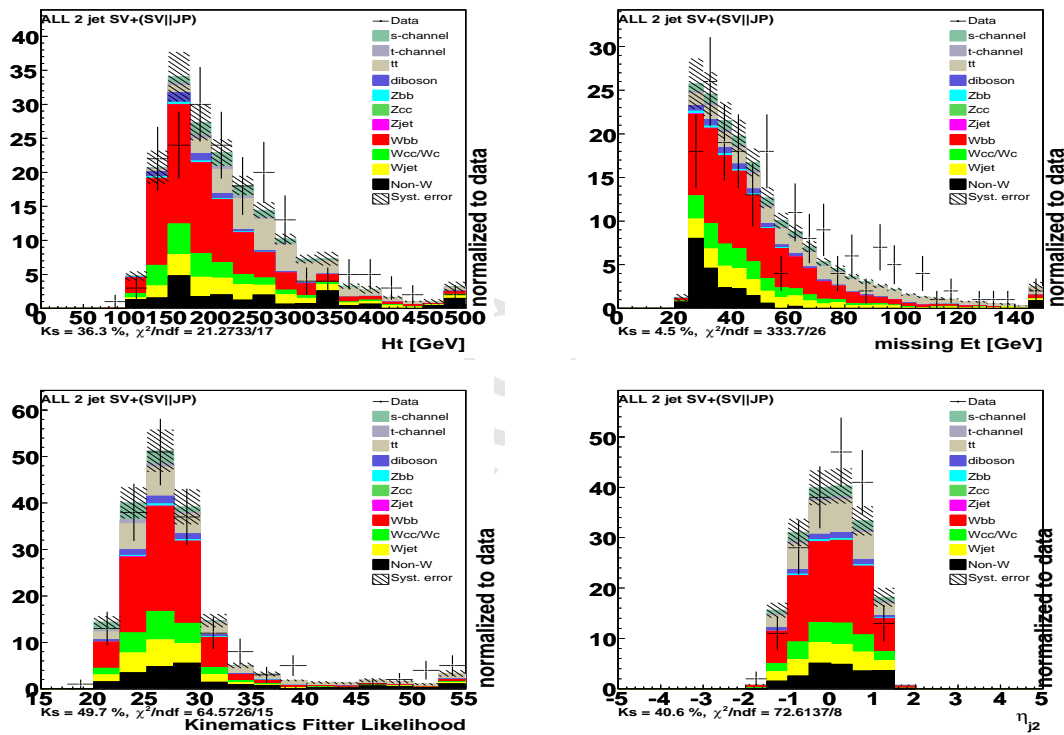


Figure 34: Input variables comparison between expected and observed. – SV + (JP||SV).

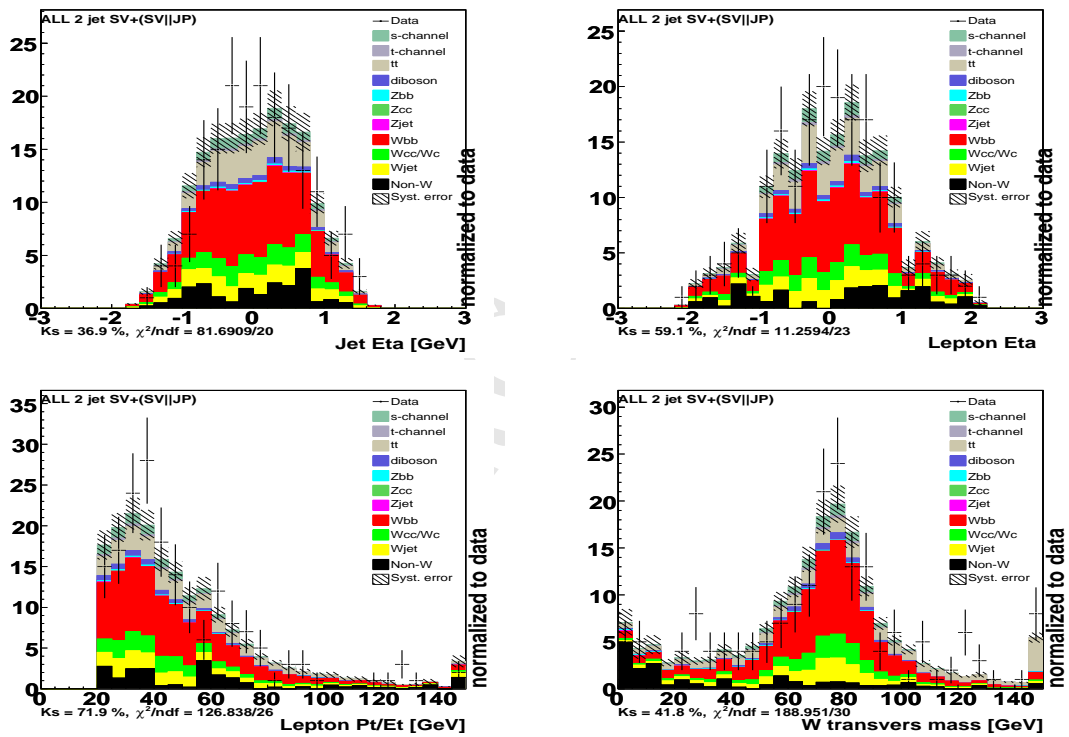


Figure 35: Input variables comparison between expected and observed. — SV + (JP||SV).

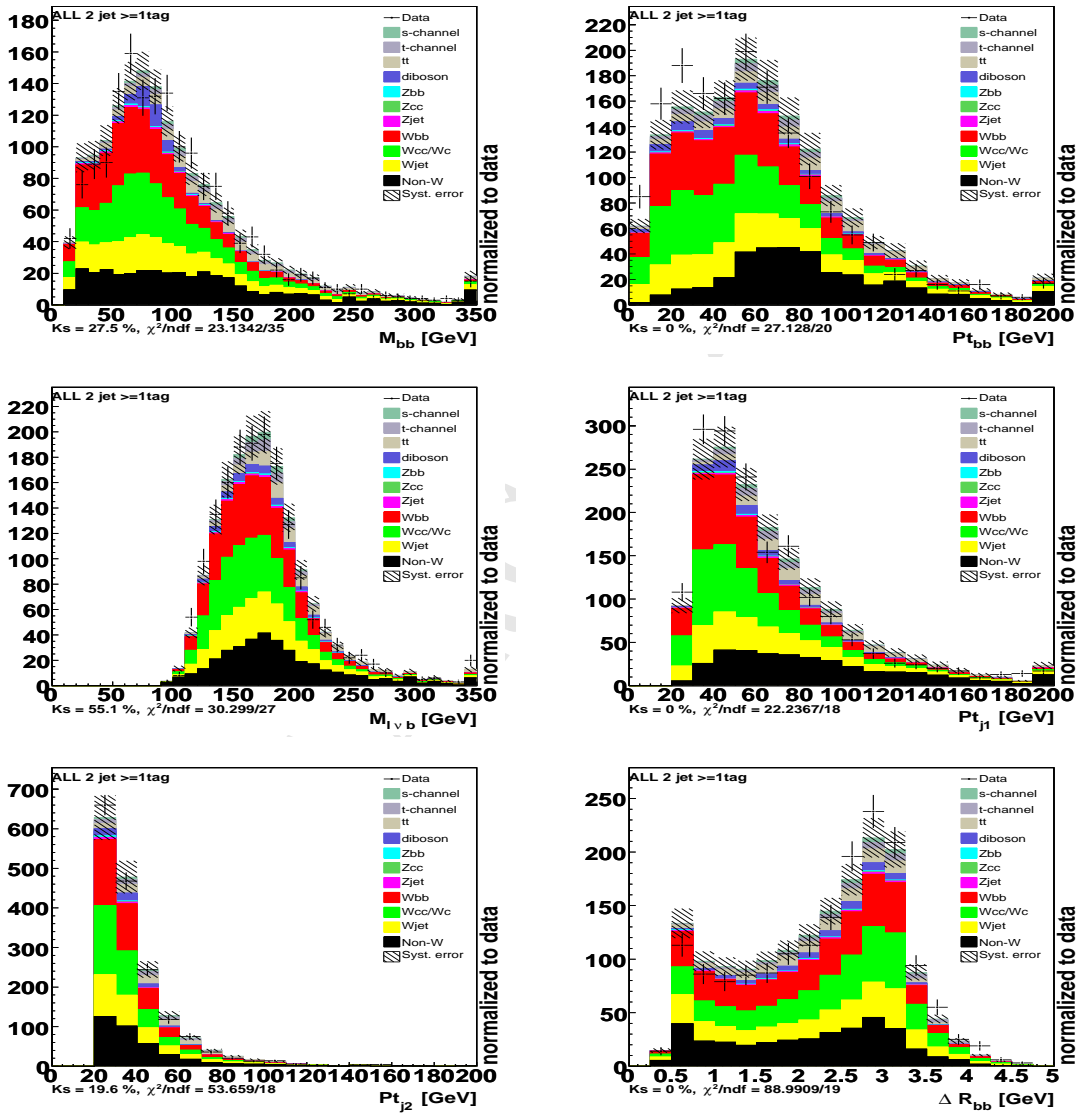


Figure 36: Input variables comparison between expected and observed. – At least 1 tag.

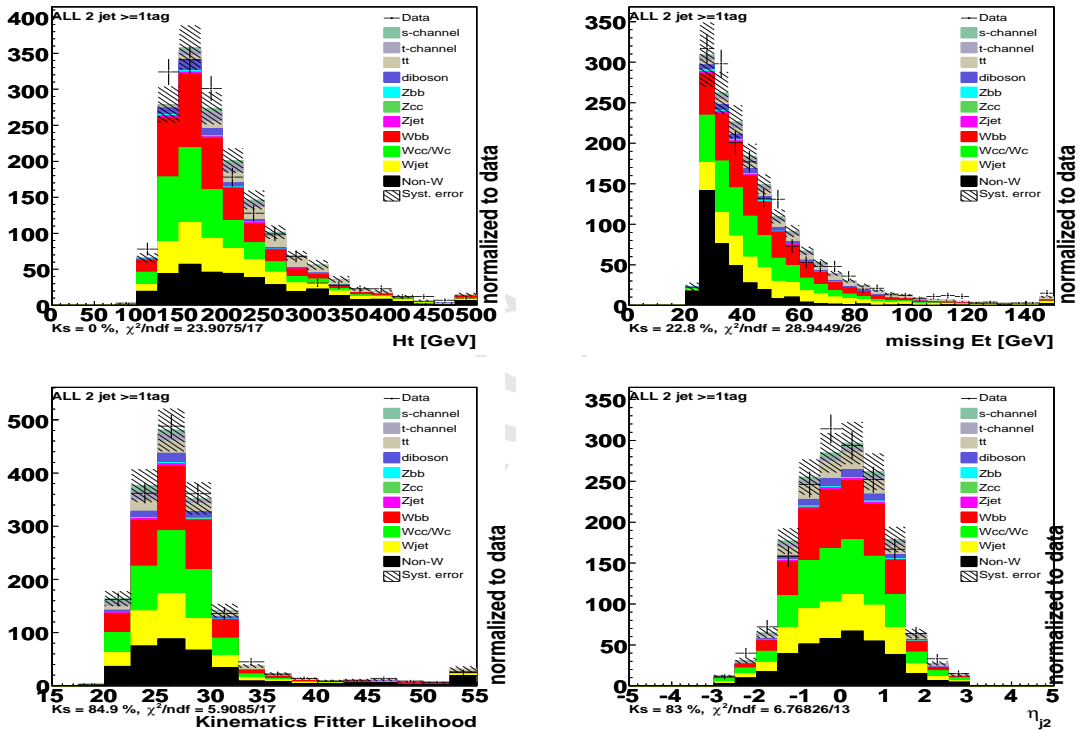


Figure 37: Input variables comparison between expected and observed. – At least 1 tag.

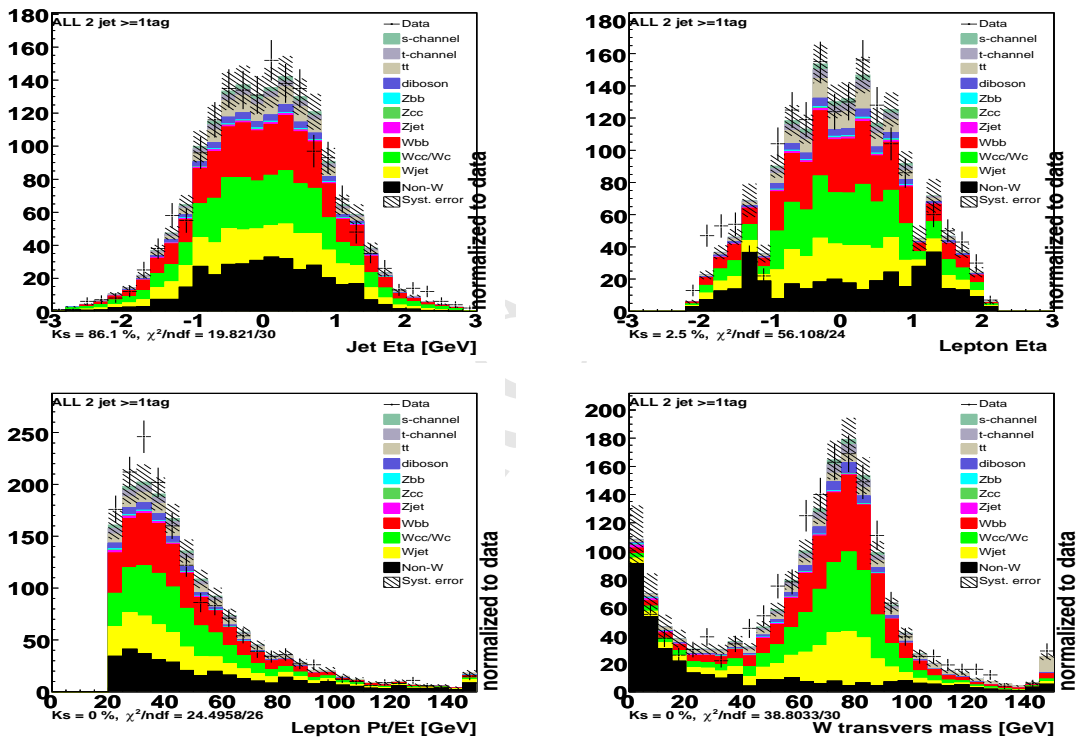


Figure 38: Input variables comparison between expected and observed. – At least 1 tag.

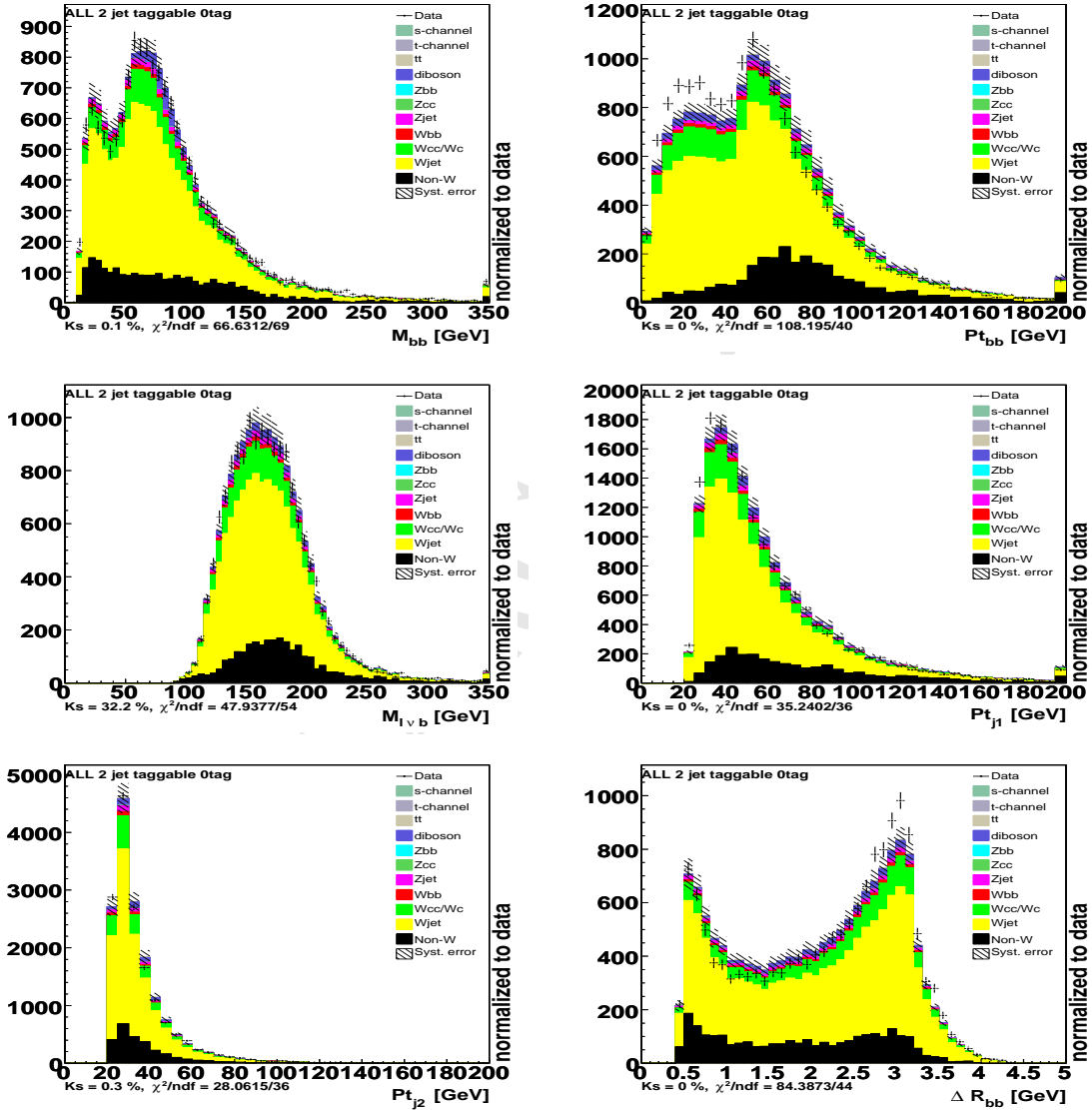


Figure 39: Input variables comparison between expected and observed. – double taggable but 0 tag .

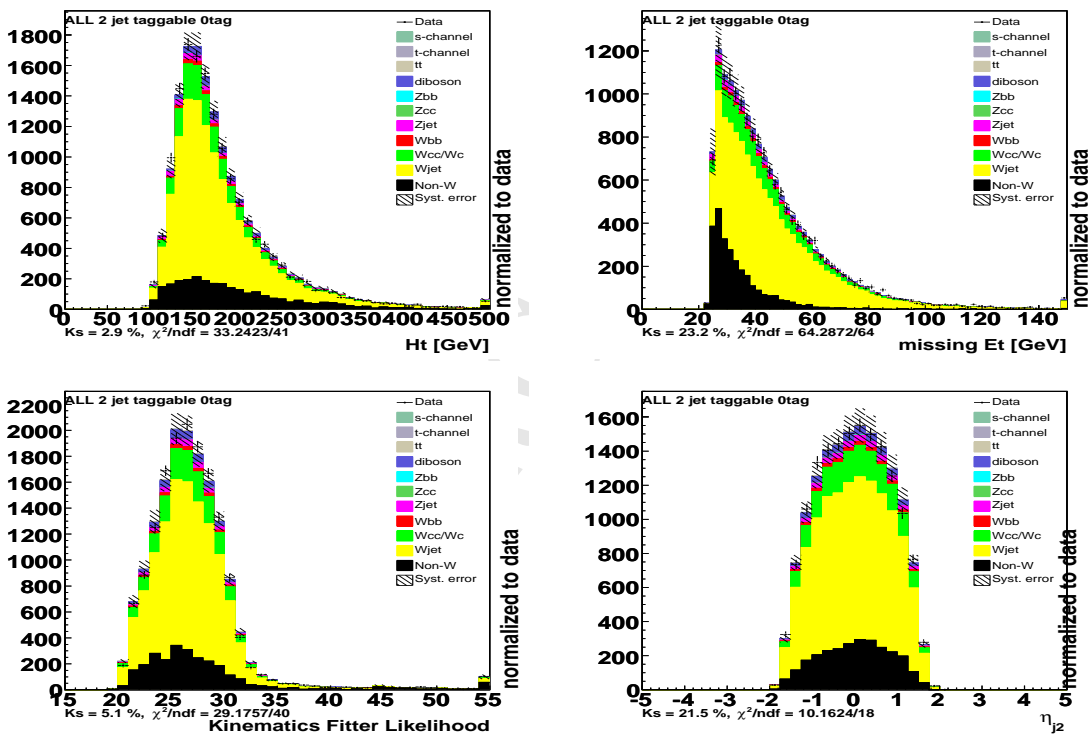


Figure 40: Input variables comparison between expected and observed. – double taggable but 0 tag .

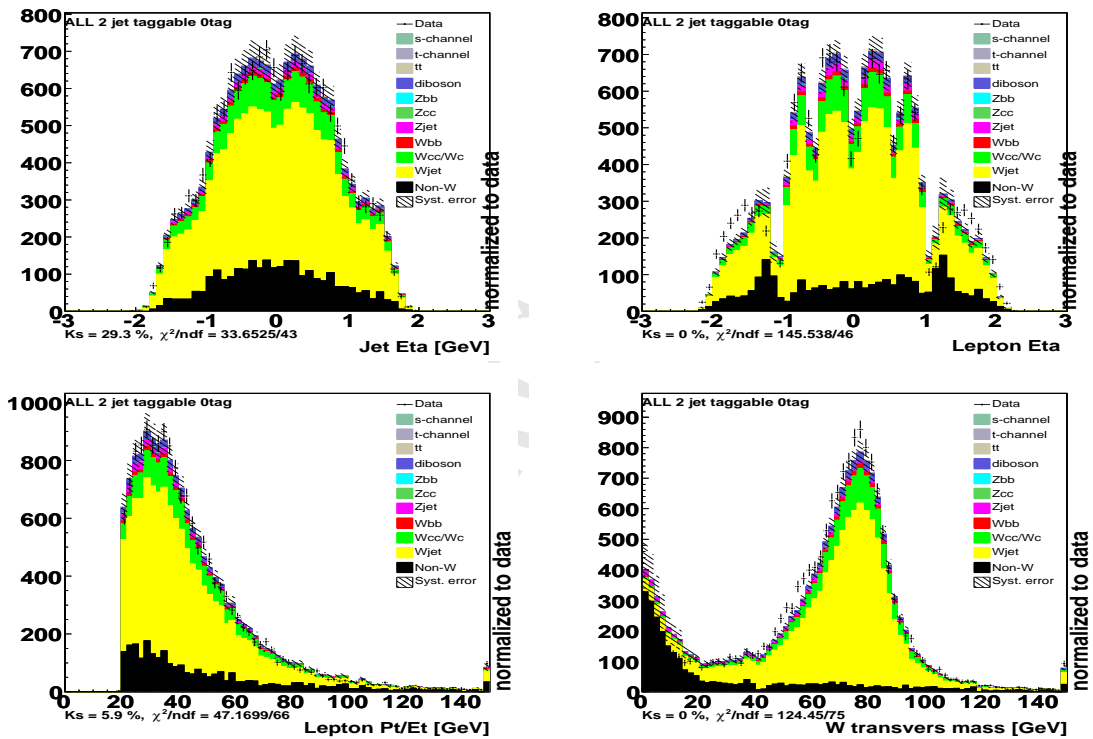


Figure 41: Input variables comparison between expected and observed. – double taggable but 0 tag .

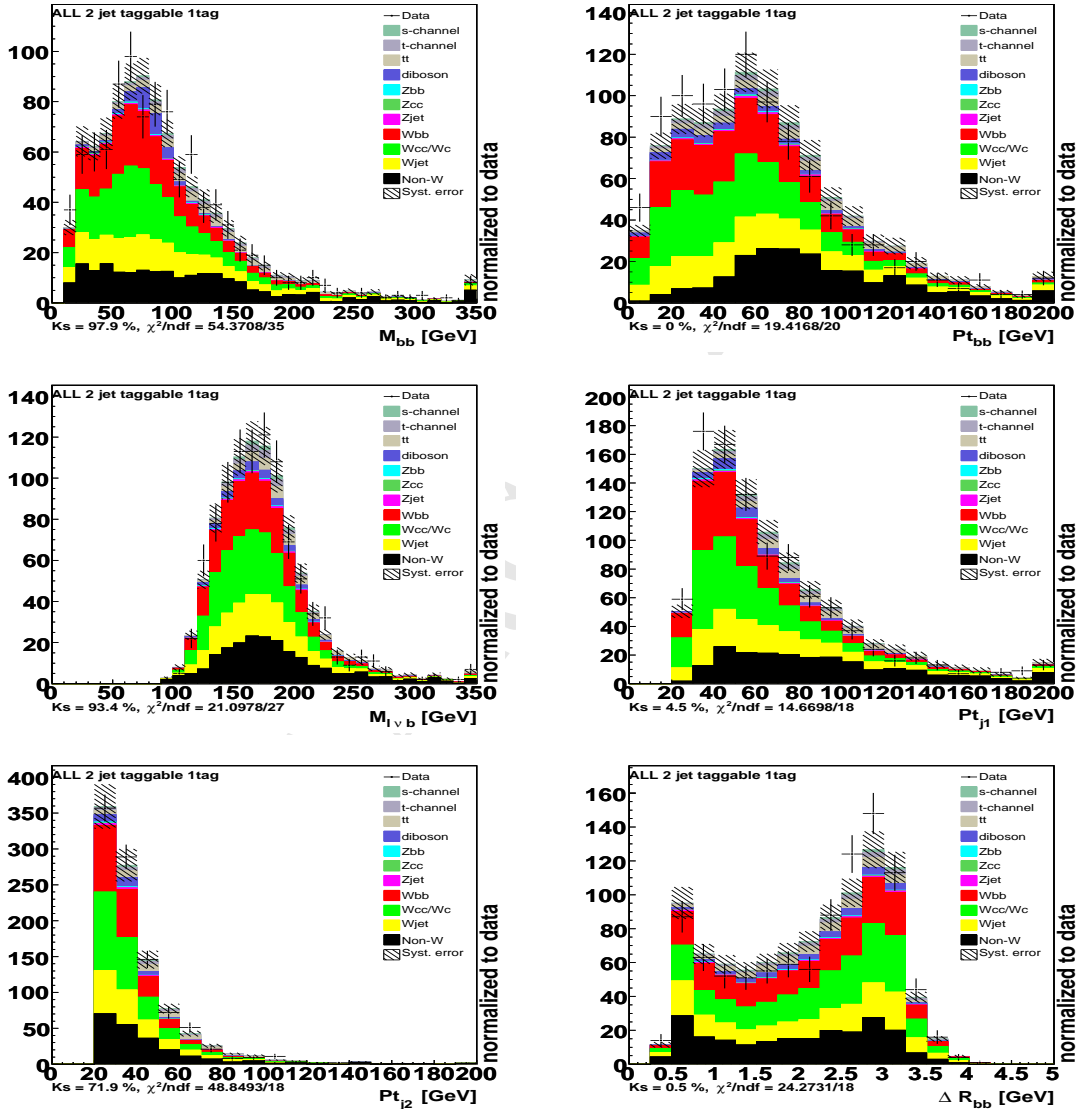


Figure 42: Input variables comparison between expected and observed. – double taggable but only 1 tag .

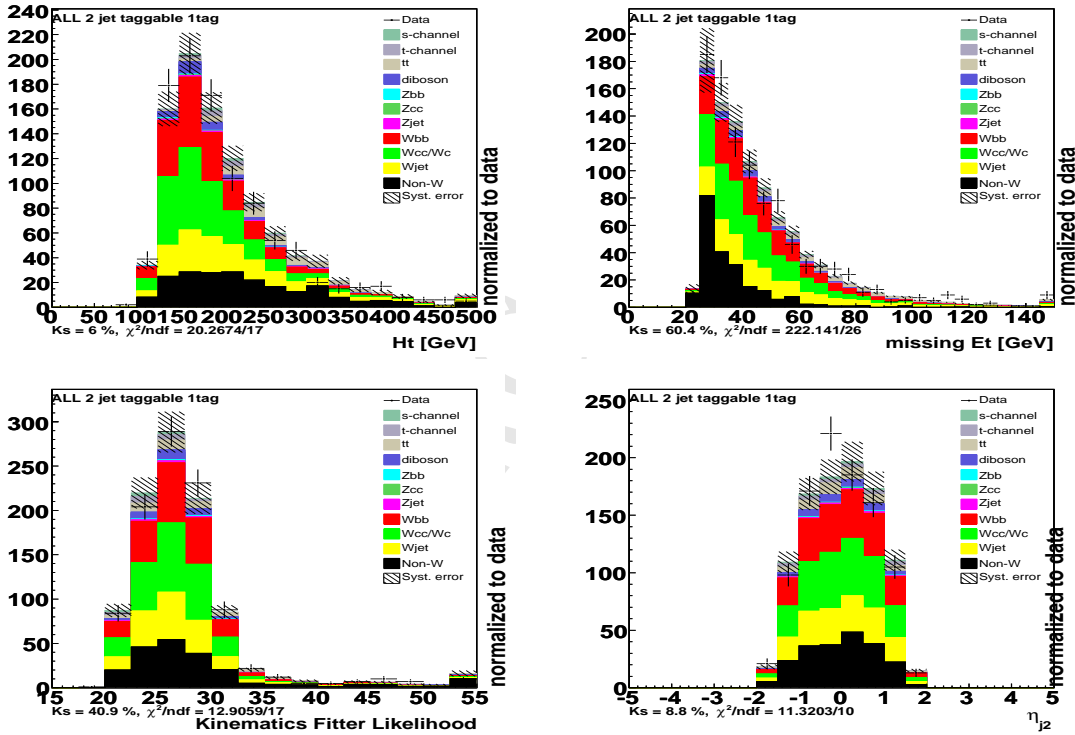


Figure 43: Input variables comparison between expected and observed. – double taggable but only 1 tag .

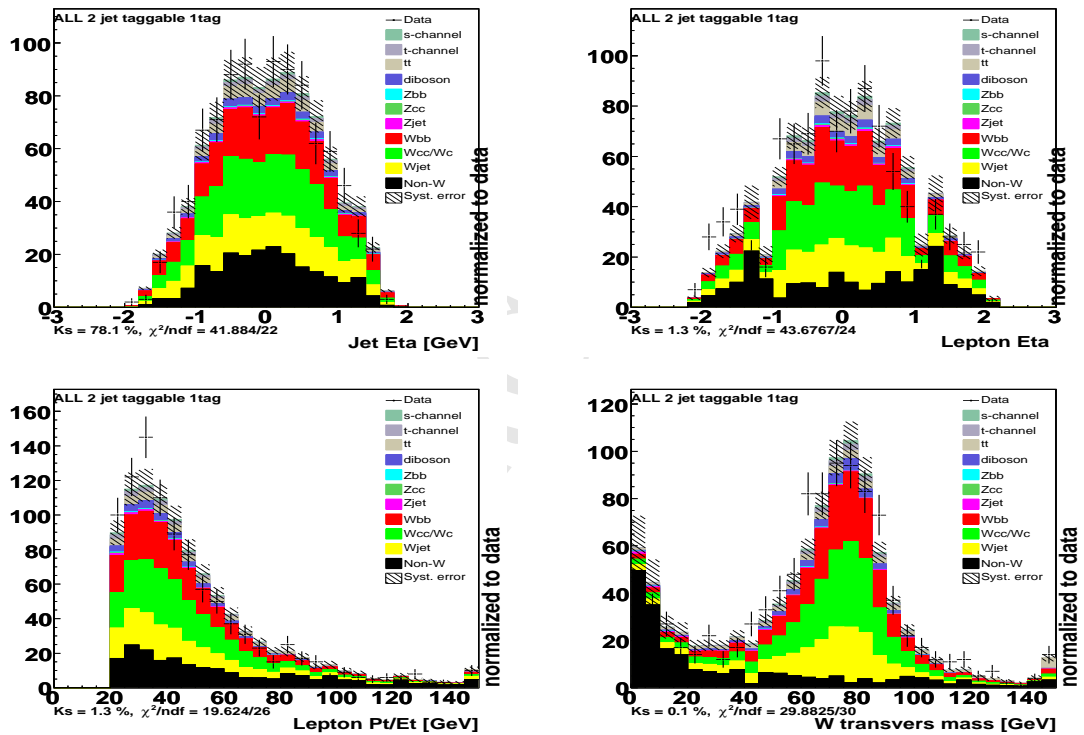


Figure 44: Input variables comparison between expected and observed. – double taggable but only 1 tag .